Journal of Power Sources 279 (2015) 1–18

Contents lists available at ScienceDirect

Journal of Power Sources

journal homepage: www.elsevier.com/locate/jpowsour

A control-oriented lithium-ion battery pack model for plug-in hybrid electric vehicle cycle-life studies and system design with consideration of health management

Andrea Cordoba-Arenas [a,*], Simona Onori [b,1], Giorgio Rizzoni [a]

[a] Center for Automotive Research and Department of Mechanical and Aerospace Engineering, The Ohio State University, Columbus, OH 43212, USA
[b] Department of Automotive Engineering, Clemson University, Greenville 29607, USA

HIGHLIGHTS

- Control-oriented methodology to model aging propagation in battery packs.
- Systematic methodology for system-level SOH assessment of battery systems.
- Pack SOH based on individual cells SOH, electrical topology and equalization approach.
- Understanding of lithium-ion battery pack aging under realistic PHEV operation.
- Capacity and power fade of battery packs containing cells with NMC-LMO cathodes.

ARTICLE INFO

Article history:
Received 25 August 2014
Received in revised form
24 November 2014
Accepted 13 December 2014
Available online 15 December 2014

Keywords:
Lithium-ion battery pack
Capacity and power fade
NMC-LMO cathodes
Aging propagation model
Cycle-life prognosis
PHEV cycling

ABSTRACT

A crucial step towards the large-scale introduction of plug-in hybrid electric vehicles (PHEVs) in the market is to reduce the cost of its battery systems. Currently, battery cycle- and calendar-life represents one of the greatest uncertainties in the total life-cycle cost of battery systems. The field of battery aging modeling and prognosis has seen progress with respect to model-based and data-driven approaches to describe the aging of battery cells. However, in real world applications cells are interconnected and aging propagates. The propagation of aging from one cell to others exhibits itself in a reduced battery system life. This paper proposes a control-oriented battery pack model that describes the propagation of aging and its effect on the life span of battery systems. The modeling approach is such that it is able to predict pack aging, thermal, and electrical dynamics under actual PHEV operation, and includes consideration of random variability of the cells, electrical topology and thermal management. The modeling approach is based on the interaction between dynamic system models of the electrical and thermal dynamics, and dynamic models of cell aging. The system-level state-of-health (SOH) is assessed based on knowledge of individual cells SOH, pack electrical topology and voltage equalization approach.

© 2014 Elsevier B.V. All rights reserved.

1. Introduction

A crucial step towards the large-scale introduction of plug-in hybrid electric vehicles (PHEVs) in the market is to reduce the cost of their energy storage devices. Lithium-ion (Li-ion) batteries are the preferred energy storage technology in PHEVs due to their high energy and power density [1]. One of the goals of U.S Department of Energy (DOE) Vehicle Technologies Program for hybrid electric systems is to, by 2022, reduce the production cost of Li-ion batteries by nearly 75% from 2012 costs. Currently, battery cycle and calendar life represents one of the greatest uncertainties in the total life-cycle cost of advanced energy storage systems [2].

A battery pack in a PHEV is a collection of modules, which are in turn made up of series/parallel combinations of individual cells. Cells are electrically connected in parallel to satisfy high capacity requirements and in series to provide the desired system voltage. Fig. 1(c,d) depicts a sketch of two possible electrical configurations [3]. The one on the left is termed PS because it consists of n_e parallel strings of m_e cells in series. The one on the right is termed SP because it consists of m_e elements in series, each consisting of n_e

* Corresponding author.
E-mail addresses: cordoba-arenas.1@osu.edu (A. Cordoba-Arenas), sonori@clemson.edu (S. Onori), rizzoni.1@osu.edu (G. Rizzoni).

[1] Part of this research was conducted at the time she was Research Scientist at OSU-CAR.

http://dx.doi.org/10.1016/j.jpowsour.2014.12.048
0378-7753/© 2014 Elsevier B.V. All rights reserved.

Nomenclature

A	heat transfer surface area [m^2]
Ah	total ampere-hour throughput [Ah]
c_p	specific heat capacity at constant pressure [Jg^{-1} K^{-1}]
C	electrical capacitance [F]
d_H	hydraulic diameter [m]
E_{aC}	cell activation energy for capacity fade [J mol^{-1}]
E_{aR}	cell activation energy for resistance growth [J mol^{-1}]
h	convective heat transfer coefficient [Wm^{-2} K^{-1}]
I	current [A]
k	thermal conductivity [Wm^{-1} K^{-1}]
L	channel length [m]
m	mass [g]
Nu	Nusselt number, hD_hk^{-1}
Pr	Prandtl number of air, 0.7023
q_{air}	volumetric flow rate of air moving through channel [m^{-3} s^{-1}]
Q	heat transfer rate [W]
R	thermal resistance [KW^{-1}] or Electrical resistance [Ohm]
Re	Reynolds number
R_g	Universal gas constant, 8.314 [JKs^{-1} mol^{-1}]
R_{inc}	battery internal resistance increase [%]
ρ	density [gm^{-3}]
S	battery capacity [Ah]
S_{loss}	capacity loss [%]
T	temperature [°C], [K]
u_{air}	velocity of main airflow [m s^{-1}]
v	kinematic viscosity [m^2 s^{-1}]
V	voltage [V]

Subscripts

air	air
c	battery cell
C	capacity fade
cc	conduction among battery cells
ch	cooling channel
i	battery cell or cooling channel index number
(j, k)	battery cell index pair
ku	surface convection
oc	open circuit
p	string of cells
$\mathscr{P}$	battery pack
R	resistance growth
s	element of cells in parallel
u	convection
0	initial or nominal conditions

superscripts

T	transpose

cells in parallel. In this paper, a string of cells in series is notated as p; while an element of cells in parallel is notated as s, see Fig. 1(a,b).

Temperature and its gradient within the battery system strongly affect battery performance, life and safety [4]. Therefore, a battery pack includes a battery thermal management system (BTM) to keep the battery at optimal average temperature, minimizing temperature differences among cells [5]. BTMs systems include: air-cooling with an electric fan [6–8]; liquid-cooling with water/glycol or refrigerants [9–11]; and liquid/solid phase change materials (PCM) [12]. Despite the fact that different thermal management strategies have been proposed for HEV/PHEV applications, air-cooled systems are still the preferred solution due to its manufacturing cost, weight, volume, safety, and operating energy consumption [6–8]. Therefore, in this work, air-cooling BTM is chosen for the model development.

Fig. 2 shows the components and arrangement of a typical air-cooled lithium-ion battery pack for PHEV applications. The battery pack mainly consist of N interconnected cells, $(N+1)$ cooling channels surrounding the cells, defector plates and cooling fan, etc. Under forced convection condition, cooling air is drawn into the battery pack through the inlet and guided into the cooling channels by the lower air deflector. Similarly, the heated air is guided out the battery pack through the upper air deflector.

Cell parameters such as battery capacity and internal resistance, varies from cell-to-cell due to manufacturing variability, different operational conditions and aging [13], [14]. In a battery pack, cell-to-cell imbalances such as voltage, capacity and state-of-charge (SOC), negatively affect the available energy of a battery system reducing their performance and life [15–17]. Therefore, a battery pack typically includes a voltage equalizer (VE). VE strategies include: active equalization techniques (AE), in which the voltages are balanced by transferring the excess of stored energy to other cells [18–21]; and passive equalization techniques (PE), in which the excess of energy is dissipated in the form of heat [15], [22].

The United States Advanced Battery Consortium (USABC) defines two operational modes for PHEVs: Charge-Depleting (CD) and Charge-Sustaining (CS) [1]. During CD the battery is depleted starting from a battery SOC of SOC$_{\text{max}}$ and until reaching a predefined SOC$_{\text{min}}$. During CS the battery SOC is kept within a window UE$_{CS}$ with an average value of SOC$_{\text{min}}$ [1], see Fig. 3. The Ratio of CD to the total operating time is defined as the ratio of t_{CD} to $(t_{CD}+t_{CS})$:

$$\text{Ratio} = (t_{CD} : (t_{CD}+t_{CS})) = \frac{t_{CD}}{t_{CD}+t_{CS}} \tag{1}$$

which indicates the fraction of time spent in CD mode over the total operation time [23]. Therefore, Ratio $=1$ corresponds to CD operation. Ratio $=0$ corresponds to CS operation. Ratios such that $0<\text{Ratio}<1$ correspond to mixed operation i.e. the total operating time is divided between CD and CS. For example, the SOC profile shown in Fig. 3 corresponds to mixed operation with a Ratio of 1/2.

Battery charging is typically done through CC-CV protocol [24]. That is, a constant current (CC) is used until the battery voltage reaches a predetermined limit, followed by a constant voltage (CV) until the current declines to a predetermined value. In this work we express the current in terms of C-rate.[2] We refer to the CC expressed in C-rate as charging rate (CR).

Aging is the reduction in performance, availability, reliability, and life span of a system or component. Generally, battery aging manifest itself in a reduction in the ability to store energy and deliver power, performance metrics correlated with loss in capacity and increase in internal resistance [25,26]. Among the micro-mechanisms of Li-ion battery aging we cite active particle loss and metal sediment or SEI film accumulation. A review of today's knowledge on the mechanics of aging in Li-ion batteries can be found in Refs. [25,27]. These physical-chemical mechanisms are enhanced by stress factors [25,26]. The stress factors for PHEV

[2] A C-rate is a measure of the rate at which a battery is charged/discharged relative to its maximum capacity. Operationally, C-rate $= I(t)/S_0$, where $I(t)$ is battery input current and S_0 is the battery nominal capacity.

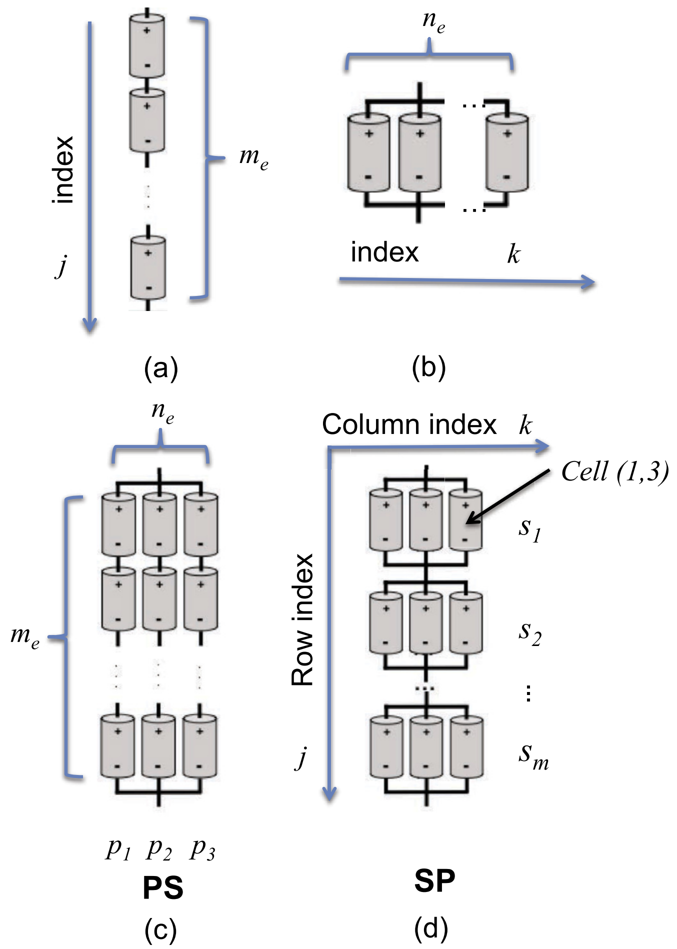

Fig. 1. (a) String of cells in series, *p*; (b) Element of cells in parallel, *s*; (c) Parallel strings of cells (PS); (d) Strings of parallel cells (SP).[3].

applications are given by Ref. [23],

- Charging rate, *CR*
- Battery skin temperature, *T*
- t_{CD} to $(t_{CD} + t_{CS})$ Ratio
- Minimum SOC, SOC_{min}

The state-of-health (SOH) of a battery cell, which is used to describe its physical condition, is commonly characterized by a cell parameter that is correlated with its aging. Depending on the application, the SOH of a battery *cell* may be characterized by loss in capacity, increase in internal resistance, or a combination of both [28],[29],[26]. The capacity and internal resistance are cell parameters correlated with be ability to store energy and deliver power respectively. In this work, we refer as capacity state of health (SOH_C) to the figure of merit that is correlated with the battery's ability to store energy; and, as power state of health (SOH_R) to the figure of merit that is correlated with the battery's ability to deliver power. In a *battery pack* the ability to store energy and deliver power, and therefore the *system level* SOH, highly depends on individual cells performance and SOH, electrical topology, and voltage equalization. From the best of our knowledge there is no work available in the literature that deals with the system level SOH assessment of interconnected systems and in particular its application to advanced battery systems.

Battery aging models are able to predict capacity and/or power loss in response to operating conditions such as C-rate, T, SOC. The field of battery aging modeling, has seen progress with respect to physics-based [30], [31] and semi-empirical models [23,2,32,33] to describe the aging of cells. However, in real world applications battery cells are interconnected and aging propagates. The propagation of aging from one cell to others exhibits itself in a reduced battery system life span. Aging propagation has a profound effect on the accuracy of battery systems SOH assessment and prognosis [34].

The field of battery *pack* modeling is sparse [13,3,35–37]. Although the field of battery modeling has seen progress in recent years, describing the battery pack life remains an open problem. In particular a model that enables the prediction of battery electro-thermal performance and life. Despite the fact that this topic has been pointed out as critical for the field of lithium ion-batteries [4,38], the problem has not yet been explored in the available literature. The complexities of battery systems make the development of efficient models and simulation tools challenging.

This paper proposes a systematic methodology for modeling the propagation of aging in advanced battery systems. The modeling approach is such that is a control-oriented multi-time scale modeling that enables the prediction of electro-thermal dynamics, aging dynamics while considering electrical topology and cell-to-cell variability. The proposed model allows for a more complete understanding of the impacts and trade-offs of cell-to-cell variability, electrical topology and battery thermal management, on battery performance and life under actual PHEV operation. The model may be also used for verification and validation of control algorithms such as estimation and identification, in particular for battery management systems including health management. This modeling approach constitutes the fist step towards an integrated system design with '*a priori*' consideration of health management.

2. Battery cell model

Fig. 5 shows a control oriented block diagram of the model of a single cell subject to aging. The model is composed of three interconnected submodels: the electrical submodel is used to predict battery cell voltage and SOC in response to current and temperature; the thermal submodel is used to predict the cell temperature in response to current, voltage and ambient temperature; and the aging submodel to predict capacity and power fade in response to the cell operating conditions charge sustaining/depleting, SOC, temperature, and charging rate.

2.1. Electrical submodel

The electrical dynamics of a battery cell are modeled by the 1st order Randle equivalent circuit model shown in Fig. 6 [39], [40]. The circuit is composed of an ideal voltage source V_{oc} to model the cell open circuit voltage, a resistance R to model the electrolyte resistance and an RC circuit in series configuration to model the cell electric dynamics (R_1, C_1). In a cell, the open circuit voltage (OCV) is defined as the voltage that is measured with a voltmeter at the terminals of a cell, when there is no current drawn into the battery.

The cell electrical model is given by:

$$\begin{aligned} \frac{dV_c(t)}{dt} &= \frac{-1}{R_1C_1}V_c(t) + \frac{I(t)}{C_1} \\ \frac{dSOC(t)}{dt} &= \frac{-I(t)}{S(t)} \\ V_{cell}(t) &= V_{oc} - R(t)I(t) - V_c(t) \end{aligned} \tag{2}$$

where $SOC(t)$ is the cell state of charge, $S(t)$ is the cell capacity, $I(t)$ is the input current, $V_c(t)$ is the voltage across the capacitor C_1 and V_{oc}

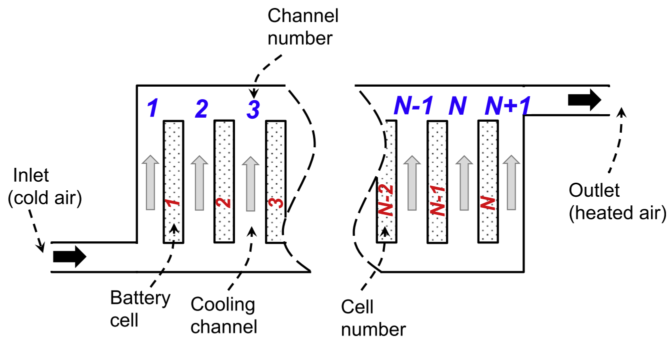

Fig. 2. Schematic view of an air-cooled battery pack.[37].

is the *OCV*. The current convention is such that negative current sign is used for charging and positive current for discharging. The *OCV* is a function of SOC and temperature. All the electrical circuit parameters depend on operating conditions (i.e current, temperature, SOC, charge/discharge), the cell capacity $S(t)$ and resistance $R(t)$ vary with the age of the battery.

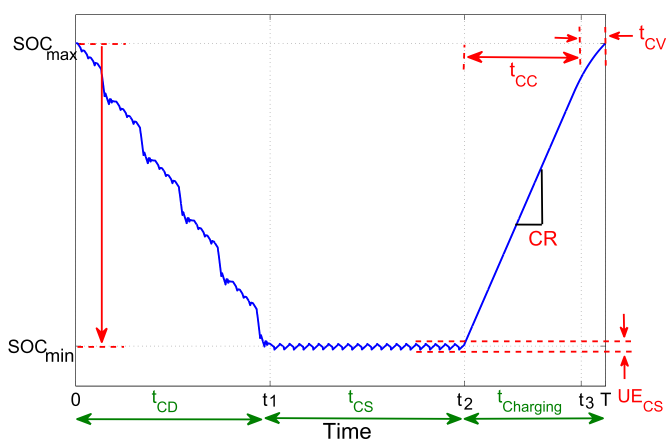

Fig. 3. Schematic of SOC profile under PHEV operation: charge depleting (CD), charge sustaining (CS) and charging.

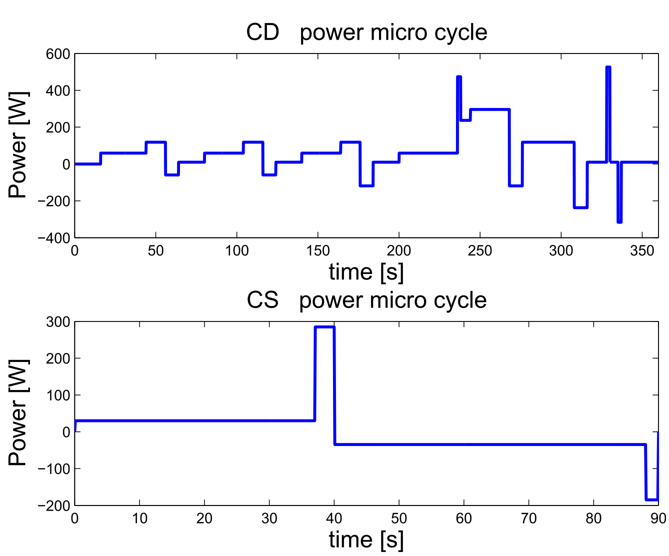

Fig. 4. Charge depliting (CD) and charge sustaining (CD) power micro-cycles.[1].

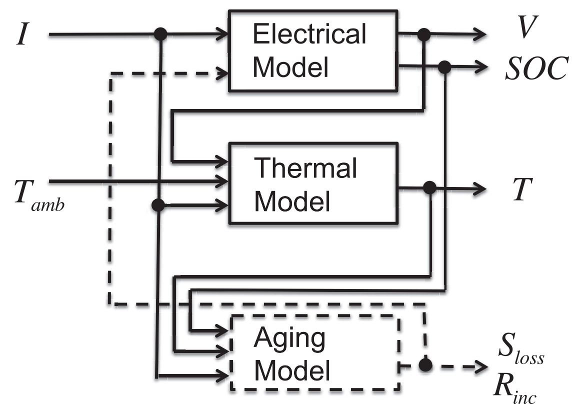

Fig. 5. Schematic of the battery cell model showing inputs and outputs.

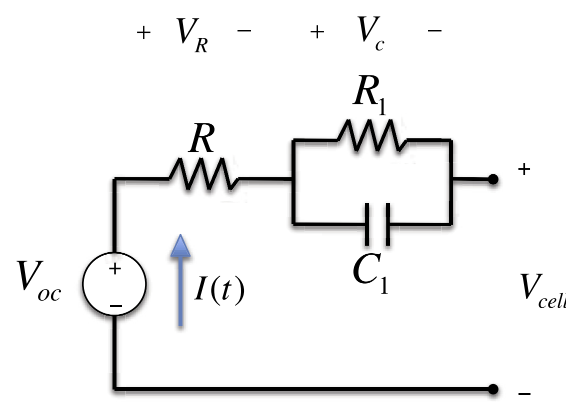

Fig. 6. Battery cell equivalent circuit model.

2.2. Thermal submodel

Fig. 7(a) shows a schematic of a lithium-ion pouch cell. For the battery cell thermal submodel, the heat generation and temperature within the cell are assumed to be uniformly distributed [41].

According to the energy conservation law, the temperature change for a single battery cell is given by:

$$m_c c_{p,c} \frac{dT}{dt} = Q_g - Q_d \tag{3}$$

where, T is the temperature within the cell; Q_g is the rate of heat generated by the single cell; and Q_d is the rate of heat removed from the cell by the cooling channels.

The rate of heat generation for a battery cell can be approximated by Ref. [42]:

$$Q_g = I \cdot \left(V_{oc} - V_{\text{cell}} - \frac{\partial V_{oc}}{\partial T} \cdot T \right) \tag{4}$$

where the dependence of the cell open circuit voltage on temperature may be neglected as a first approximation [40].

The rate of heat dissipated by the cooling channels is given by:

$$Q_d = Q_{ku,1} + Q_{ku,2} \tag{5}$$

where, $Q_{ku,1}$ and $Q_{ku,2}$ are the rate of heat removed from the cell by the cooling channels 1 and 2 respectively.

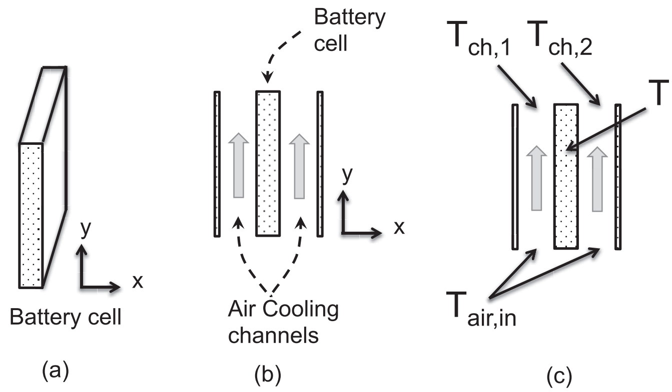

Fig. 7. Schematic view of (a) a battery cell, (b) battery cell and cooling channels, (c) battery cell and cooling channel notation.

Heat is removed from the battery cell by surface convection, when air enters the channel at a uniform temperature less than the battery temperature. For a rectangular channel with constant wall temperature, the local heat transfer coefficient can be estimated using the analytical correlation for laminar forced convection proposed in Ref. [43] as.

$$h(y) = \frac{6 \cdot k_{air}}{d_H} \sqrt[3]{\frac{Re \cdot Pr \cdot d_H}{120 \cdot y}} \tag{6}$$

where, k_{air} is the air thermal conductivity and d_H is the cooling channel hydraulic diameter, Pr is the Prandtl number of air, y is the channels longitudinal coordinate value and, the Reynolds number is given by

$$Re = \frac{u_m \cdot d_H}{\nu_{\mathrm{air}}} \quad u_m = \frac{2 \cdot u_{\mathrm{air}}}{3} \tag{7}$$

Since the cooling channel length is much larger that its hydraulic diameter (i.e. $L_{ch} \gg d_H$), we can say that the fully developed region length is much larger than the thermal entrance region length, and we can simplify the model by making the reasonable assumption that the local convection coefficient is approximately constant along the cooling channel and takes the value of the average local heat transfer coefficient over the length of the channel, $\overline{h}$. Therefore,

$$\overline{h} = \frac{\int_0^{L_{ch}} h(y)dy}{L_{ch}} \tag{8}$$

Since the local heat transfer coefficient is higher at the inlet of the channel and channel's mean temperature is rapidly increases along the channel, the air temperature at the outlet of the channel is used to express the rate of heat removed by surface convection. Therefore, the rate of heat removed by surface convection by the cooling channel (index number i, $i = 1{,}2$) can be expressed using Newton's law of cooling as.

$$Q_{ku,i} = \overline{h_i} \cdot A_{ch} \cdot (T - T_{ch,i}) \tag{9}$$

where, A_{ch} is the cooling channel heat transfer surface area and, $T_{ch,i}$ is the air temperature at the outlet of channel i.

The energy balance equation for the air stream flowing through the channel (index number i, $i = 1{,}2$) is given by.

$$Q_{ku,i} - Q_{u,i} = 0 \tag{10}$$

where,

$$Q_{u,i} = \rho_{\mathrm{air}} \cdot c_{p,\mathrm{air}} \cdot q_{\mathrm{air},i} (T_{ch,i} - T_{\mathrm{air},i}) \tag{11}$$

A schematic of the thermal circuit diagram for a single cell is shown in Fig. 8.

The estimation of convection heat transfer rate between battery cooling surface and cooling air and other parameters can be verified by measuring battery cooling plate temperature changes following

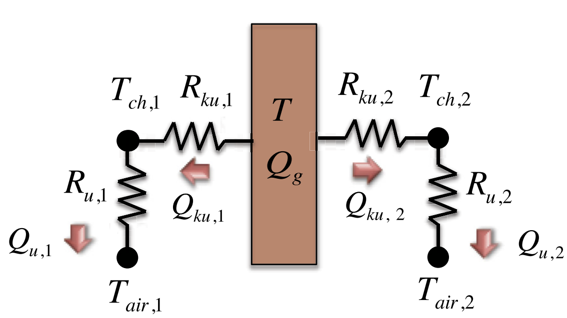

Fig. 8. Thermal circuit diagram for an isolated (i.e not interconnected) battery cell.

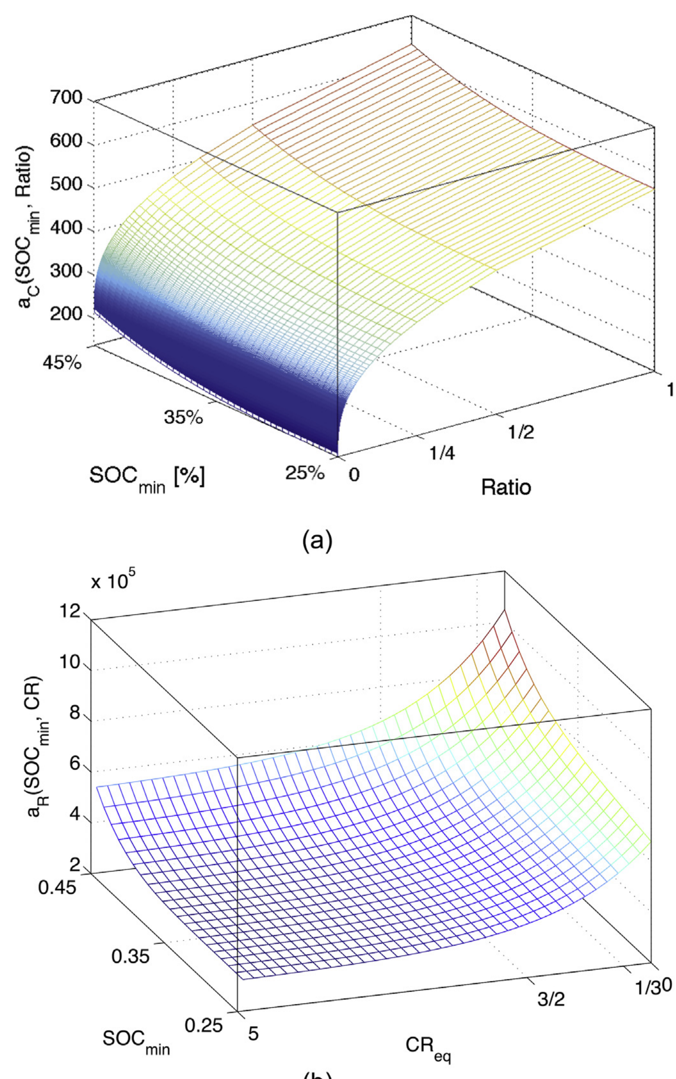

Fig. 9. Severity factor (SF) surfaces for an LMO-NMC Lithium-ion battery cell: (a) Capacity SF (Equation (14)) (b) Resistance SF (Equation (18))[23].

a designated testing procedure such as the one proposed in Refs. [36], [44] using a CFD model such as the one proposed in Refs. [7], [36] or using system identification techniques [45]. Similarly, the proposed methodology can be used for liquid-cooled TMS by estimating the corresponding parameters using similar approaches as the ones previously mention. For example, in Ref. [46] a CFD model is used to calculate the flow rate and pressure drop on channels in a fluid cooling system.

2.3. Aging submodel

The aging submodel describes the capacity and power fade as function of the influencing PHEV stress factors and the battery charge throughput [23]. In a battery, the total ampere-hour throughput [Ah] in both charge and discharge is given by $Ah = \int_0^t \left| I(\tau) \right| \mathrm{d}\tau$, where $I(t)$ is the input current to the battery [47]. The aging submodel is composed of two elements: the capacity fade model and a resistance growth model.

2.3.1. Capacity fade

The cell capacity loss [%] after $Ah > 0$ charge throughput is given as;

$$S_{\mathrm{loss}}(Ah) = 100 \cdot \frac{S_0 - S(Ah)}{S_0} \tag{12}$$

where S_0 is the cell nominal capacity and $S(Ah)$ is the cell capacity after $Ah > 0$ charge throughput. The capacity loss of a single cell is described by Ref. [23],

$$S_{\mathrm{loss}}(Ah) = a_C(SOC_{\mathrm{min}}, \mathrm{Ratio}) \cdot \exp\left(\frac{-E_{a_C}}{R_g T}\right) \cdot Ah^z \tag{13}$$

where, $a_C(\cdot)$ is the capacity severity factor function given by,

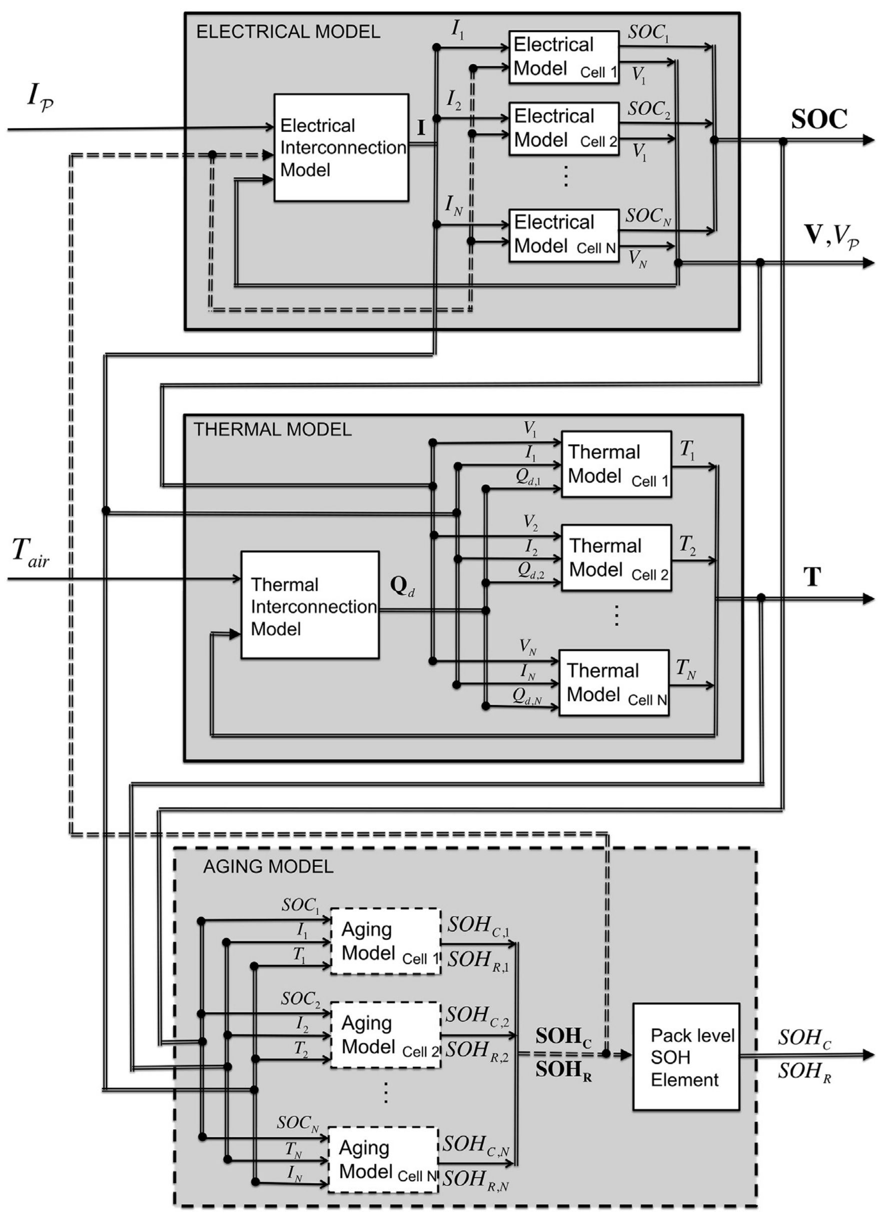

Fig. 10. Schematic of the battery pack model showing inputs and outputs.

$$a_C(\cdot) = \alpha_C + \beta_C \cdot (\text{Ratio})^b + \gamma_C \cdot (SOC_{\min} - SOC_0)^c \tag{14}$$

where the dimensionless constant coefficients α_C,β_C,γ_C,b,c,z, SOC_0, and the dimensional constant coefficient E_{aC} are obtained from experimental data. Fig. 9(a) shows the surface $a_C(\cdot)$ that describes the dependence of capacity fade on $SOC_{\min}$ and Ratio.

We adopt the definition of the battery cell capacity state of health as the ratio of the cell capacity at ampere-hour throughput $Ah > 0$ to the cell nominal capacity S_0. Therefore, the SOH_C of a cell is given by:

$$SOH_C(Ah) = \frac{100 - S_{loss}(Ah)}{100} \tag{15}$$

For a fresh cell, the capacity state of health is equal to one ($SOH_C = 1$) and decreases with aging. For automotive applications, from a capacity stand point, the cell end-of-life (EOL) is reached when the SOH_C reaches 0.8 (i.e. 20% of capacity loss).

2.3.2. Resistance growth

The resistance growth [%] after $Ah > 0$ charge throughput is given by Ref. [23]:

$$R_{\text{inc}}(Ah) = 100 \cdot \frac{R(Ah) - R_0}{R_0} \tag{16}$$

where R_0 is the cell nominal internal resistance and $R(Ah)$ is the cell internal resistance after $Ah > 0$ charge throughput. The resistance growth of a single cell is described by:

$$R_{inc}(Ah) = a_R(SOC_{\min}, \text{Ratio}, CR) \cdot \exp\left(\frac{-E_{aR}}{R_g T}\right) \cdot Ah \tag{17}$$

where $a_R(\cdot)$ is the resistance severity factor function given by:

$$a_R(\cdot) = \alpha_R + \beta_R \cdot (SOC_{\min} - SOC_0)^{c_R} + \gamma_R \cdot \exp\left[d \cdot (CR_0 - CR_{eq}) + e \cdot (SOC_{\min} - SOC_0)\right] \tag{18}$$

where CR_{eq} is a function of Ratio given by:

$$CR_{eq}(\text{Ratio}) = \begin{cases} 0 & \text{Ratio} = 0 \\ CR & \text{Ratio} > 0 \end{cases} \tag{19}$$

and, the dimensionless constant coefficients α_R,β_R,γ_R,c_R,d,e, SOC_0 and the dimensional constant coefficient E_{aR} are obtained from experimental data. Fig. 9(b) shows the resistance severity factor surface $a_R(\cdot)$ that describes the dependence of resistance growth on $SOC_{\min}$ and CR_{eq}.

In extended-range PHEV applications, high power and high capacity to store energy are required. Therefore in addition to capacity loss, the SOH needs to be characterized with a system parameter correlated with power fade. The internal resistance is commonly used as a cell parameter correlated with power loss [28,29]. For this reason, we define the power SOH of a single cell as the ration of the cell internal resistance at ampere-hour throughput $Ah > 0$ to the cell nominal resistance R_0. Therefore, the SOH_R of a cell is given by.

$$SOH_R(Ah) = \frac{100 + R_{inc}(Ah)}{100} \tag{20}$$

For a fresh cell, the power SOH is equal to one ($SOH_R = 1$) and increases with aging. For automotive applications from a power performance stand point, the cell end-of-life (EOL) of a battery is reached when the SOH_R reaches 1.2 (i.e. 20% in resistance increase, approximately 20% in power loss).

2.3.3. Aging submodel dynamics

Combining the two aging elements described before, the aging dynamics for a single cell are given by:

$$\begin{bmatrix} \dfrac{dSOH_C}{d(Ah)} \\ \dfrac{dSOH_R}{d(Ah)} \end{bmatrix} = \begin{bmatrix} \phi_1(w) \cdot Ah^{z-1} \\ \phi_2(w) \end{bmatrix} \tag{21}$$

where:

$$\begin{aligned} \phi_1(w) &= -\frac{z}{100} \cdot a_C(SOC_{\min}, \text{Ratio}) \cdot \exp\left(\frac{-E_{a_C}}{R_g T}\right) \\ \phi_2(w) &= \frac{1}{100} \cdot a_R(SOC_{\min}, \text{Ratio}, CR) \cdot \exp\left(\frac{-E_{aR}}{R_g T}\right) \\ w &= [SOC_{\min}, \text{Ratio}, CR, T] \end{aligned} \tag{22}$$

2.4. Battery cell model

Combining the three submodels previously described, a battery cell subject to aging can be described by *fast dynamics* coupled with *slow or aging dynamics* [47],

$$\begin{aligned} \dot{x}(t) &= \begin{bmatrix} \dot{V}_c \\ \dot{SOC} \\ \dot{T} \end{bmatrix} = \begin{bmatrix} \dfrac{-1}{R_1 C_1} V_c + \dfrac{I}{C_1} \\ \dfrac{-I}{SOH_C \cdot S_0} \\ \dfrac{I(I \cdot SOH_R \cdot R_0 - V_c)}{m_c c_{p,c}} - \dfrac{(\alpha_1 T + \alpha_2 T_{air,1} + \alpha_3 T_{air,2})}{m_c c_{p,c}} \end{bmatrix} \\ \frac{dSOH}{d(Ah)} &= \begin{bmatrix} \dfrac{dSOH_C}{d(Ah)} \\ \dfrac{dSOH_R}{d(Ah)} \end{bmatrix} = \begin{bmatrix} \phi_1(w) \cdot Ah^{b-1} \\ \phi_2(w) \end{bmatrix} \\ y(t) &= [V] = V_{oc} - SOH_R \cdot R_0 \cdot I - V_c \\ Ah &= \int_0^t \left| I(\tau) \right| d\tau \end{aligned} \tag{23}$$

where:

- $x(t) \in \mathbb{R}^3$ is the set of state variables associated with the fast dynamic behavior of the cell which correspond to the electrical and thermal dynamics;
- $SOH(Ah) \in \mathbb{R}^2$ is the set of variables that describe the state of health the cell: the capacity state-of-health $SOH_C(Ah)$ and the power state-of-health $SOH_R(Ah)$ (slowly vary with aging);
- $I(t) \in \mathbb{R}$ and $T_{air,i}(t) \in \mathbb{R}$ are the inputs acting on the cell;
- $w \in \mathbb{R}^4$ is the set of stress factors given by $w = [SOC_{\min}, \text{Ratio}, CR, T]$;
- $V \in \mathbb{R}$ is the cell output;
- $\phi_1(w)$ and $\phi_2(w)$ are nonlinear functions given by Equation (22).
- α_1, α_2, α_3 are system parameters given by $\alpha_1 = \frac{1}{R_{ku,1}+R_{u,1}} + \frac{1}{R_{ku,2}+R_{u,2}}$, $\alpha_2 = \frac{-1}{R_{ku,1}+R_{u,1}}$, $\alpha_3 = \frac{-1}{R_{ku,2}+R_{u,2}}$;

- $R_{ku,i} = \frac{1}{h_i A_{ch}}$, $R_{u,i} = \frac{1}{\rho_{air} c_{p,air} q_{air,i}}$.

3. Battery pack model

Fig. 10 shows a control oriented block diagram of the model of a battery *pack* composed of N battery cells subject to aging. The model is composed of three interconnected submodels: the electrical submodel is used to predict battery cells voltages and SOCs in response to pack current and ambient temperature; the thermal submodel is used to predict cells temperatures in response to cells currents, voltages and ambient temperature; and the aging submodel to predict battery cells capacity and power fade in response to the cells operating conditions charge sustaining/depleting, SOC, temperature, charging rate.

With respect to the location of a cell within the cooling arrangement, each cell is notated with an index number (i) such that $i \in \mathscr{I} = \{1 \le i \le N\}$, where N is the total number of cells in the pack, see Fig. 2. With respect to the location of a cell within the electrical arrangement, each cell is notated with a index order pair (j,k) such that $(j,k) \in (\mathscr{J} \times \mathscr{K})$, where $\times$ is the Cartesian product, $\mathscr{J} = \{1 \le j \le m_e\}$, $\mathscr{K} = \{1 \le k \le n_e\}$, n_e is the total number of columns, m_e is the total number of rows in the electrical arrangement, and $N = n_e \cdot m_e$, see Fig. 1. For PS topology, the k-th parallel string of cells is series is notated as p_k. For SP topology, the j-th element in series is notated as s_j. We defined the bijective function $f_{(i)\leftrightarrow(j,k)} : \mathscr{I} \leftrightarrow (\mathscr{J} \times \mathscr{K})$ which maps the cooling arrangement set of index numbers $\mathscr{I}$ to the electrical arrangement set of index pairs $(\mathscr{J} \times \mathscr{K})$. Therefore, a battery pack $\mathscr{P}$ is notated as $\mathscr{P}(n_e, m_e, \mathscr{T}_e, VE, f_{(i)\leftrightarrow(j,k)})$ where $\mathscr{T}_e \in \{SP, PS\}$ and $VE \in \{AE, PE\}$.

We refer as $Ah_{\mathscr{X}}$, where $\mathscr{X} \in \{i, (j,k), p, s, \mathscr{P}\}$, to the *cell*, *string*, *element* or *pack* ampere-hour throughput at time t, respectively. Where $Ah_{\mathscr{X}}$ is defined as:

$$Ah_{\mathscr{X}} = \int_0^t \left| I_{\mathscr{X}}(\tau) \right| d\tau \tag{24}$$

where, $I_{\mathscr{X}}(t)$ is the *cell*, *string*, *element* or *pack* input current respectively.

This section describes the fast and slow dynamics of a battery module/pack.

3.1. Electrical submodel

The electrical submodel is composed of $N+1$ elements: N cell electrical elements are used to predict battery cells voltages and SOCs in response to cells input currents; and the electrical interconnection model is used to predict the input current to the cells in response to battery input power/current.

3.1.1. Electrical elements

Each cell in the pack is modeled by a 1st order Randle model

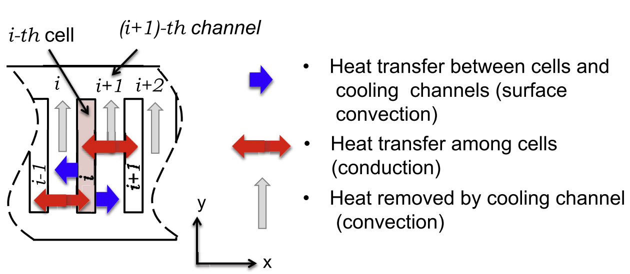

Fig. 11. Schematic of the thermal model heat transfer modes.

(Equation (2)). To model manufacturing variability, within each cell the parameters resistance R and capacity S are assumed to be normally distributed [3]. Therefore, for a cell index order pair (j,k), the parameters are varied using the following expression.

$$\begin{aligned} R_{v,(j,k)} &= SOH_{R,(j,k)} \cdot r_{R,(j,k)} \cdot R_{b,(j,k)} \\ S_{v,(j,k)} &= SOH_{C,(j,k)} \cdot r_{C,(j,k)} \cdot S_{b,(j,k)} \end{aligned} \tag{25}$$

where, $R_{b,(j,k)}$ and $S_{b,(j,k)}$ are the base scheduled parameters resistance and capacity respectively, $SOH_{R,(j,k)}$ is the cell power state of health, $SOH_{C,(j,k)}$ is the capacity state of health, $r_{R,(j,k)} \sim \mathscr{N}(1, \sigma_R)$, $r_{C,(j,k)} \sim \mathscr{N}(1, \sigma_C)$, $r_{(j,k)}$ are a normally distributed numbers, σ_C, σ_R are the standard deviations for the capacity and internal resistance respectively, $R_{v,(j,k)}$ and $S_{v,(j,k)}$ are the resulting varied scheduled parameters. For simplicity, for the rest of the discussion, σ_C and σ_R are assumed to be the equal, and equal to σ.

3.1.2. Electrical interconnection element

The input current $I_{(j,k)}$ for a cell index order pair (j,k), is calculated using Kirchhoffs voltage and current laws. For each electrical topology, $I_{(j,k)}$ is calculated in terms of the battery pack input current $I_{\mathscr{P}}$ and cells electrical parameters. Therefore, the electrical interconnection element (EIE) for a module $\mathscr{P}(n_e, m_e, \mathscr{T}_e, f_{(i)\leftrightarrow(j,k)})$ is given by the following linear set of equations:

$$\begin{aligned} \mathbf{A}_{\mathscr{T}_e} \cdot \mathbf{I} &= \mathbf{B}_{\mathscr{T}_e} \cdot [\mathbf{V_{oc}} - \mathbf{V_c}] + \mathbf{C}_{\mathscr{T}_e} \cdot I_{\mathscr{P}} \\ I_{\mathscr{P}} &= \frac{P_{\mathscr{P}}}{V_{\mathscr{P}}} \end{aligned} \tag{26}$$

where:

- $I_{\mathscr{P}}(t) \in \mathbb{R}$ is the pack input current;

The set of inputs to the EIE are:

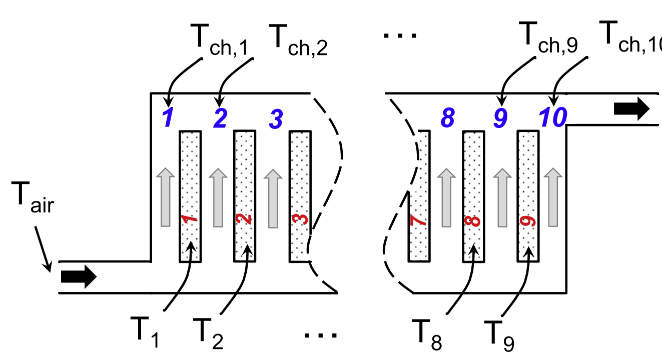

Fig. 12. Nomenclature for the lumped-capacitance thermal modeling, $N = 9$.

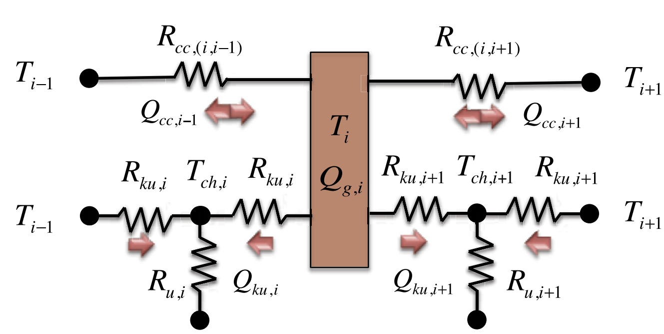

Fig. 13. Thermal circuit diagram for a battery cell (index number, $2 \le i \le N-1$).

- $P_{\mathscr{P}}(t) \in \mathbb{R}$ is the pack input power request;
- $V_{\mathscr{P}}(t) \in \mathbb{R}$ is the pack output voltage;
- $\mathbf{V_{oc}}(t) \in (\mathbb{R}^N \times 1)$, is the vector of cells OCVs,

$$\mathbf{V_{oc}}(t) = \left[V_{oc,1}(t), V_{oc,2}(t), \ldots, V_{oc,N-1}(t), V_{oc,N}(t)\right]^T$$

- $\mathbf{V_c} \in (\mathbb{R}^N \times 1)$ is the vector of cells voltages across the capacitor,

$$\mathbf{V_c}(t) = \left[V_{c,1}(t), V_{c,2}(t), \ldots, V_{c,N-1}(t), V_{c,N}(t)\right]^T$$

the EIE output is:

- $\mathbf{I} \in (\mathbb{R}^N \times 1)$, is the vector of input currents at the cells.

$$\mathbf{I}(t) = [I_1(t), I_2(t), \ldots, I_{N-1}(t), I_N(t)]^T$$

and the EIE system parameters are:

- $A_{\mathscr{T}_e}(\sigma, \mathrm{SOH_R}) \in (\mathbb{R}^N \times \mathbb{R}^N), B_{\mathscr{T}_e} \in (\mathbb{R}^N \times \mathbb{R}^N)$ and $C_{\mathscr{T}_e} \in (\mathbb{R}^N \times 1)$, are the matrices which entries depend on $n_e, m_e, \mathscr{T}_e, f_{(i)\leftrightarrow(j,k)}, \mathrm{SOH_R}$, and are given by,

$$(\mathbf{A}_{\mathscr{T}_e}, \mathbf{B}_{\mathscr{T}_e}, \mathbf{C}_{\mathscr{T}_e}) = \begin{cases} \text{Equations (47)} & \text{if } \mathscr{T}_e = SP \\ \text{Equations (48)} & \text{if } \mathscr{T}_e = PS \end{cases}$$

where $R_{v,(j,k)}$ is given by Equation (25) and $\mathbf{SOH_R} = [SOH_{R,1}, SOH_{R,2}, \ldots, SOH_{R,N-1}, SOH_{R,N}]$. See appendix for equations (47), (48).

3.2. Thermal submodel

The thermal submodel is composed of $N + 1$ elements: N cell thermal elements that are used to predict cell temperature in response to cell input current, cell output voltage and heat dissipated from the cell; and the thermal interconnection model is used to predict the heat dissipated from the cells in response to battery cells temperatures and air input temperature.

3.2.1. Thermal elements

The temperature change for a battery cell (index number i, $1 \le i \le N$) is modeled according to the energy conservation law (Equation (3)).

$$m_c c_{p,c} \frac{dT_i}{dt} = Q_{g,i}(t) - Q_{d,i}(t) \tag{27}$$

where, $Q_{g,i}(t)$ is the rate of heat generated by the cell (index number i), and $Q_{d,i}(t)$ is given by:

$$\begin{aligned} Q_{d,i}(t) = Q_{cc,(i,i-1)}(t) - Q_{cc,(i,i+1)}(t) \\ + Q_{ku,(i,i)}(t) + Q_{ku,(i,i+1)}(t) \end{aligned} \tag{28}$$

where: $Q_{cc,(i,i-1)}$ and $Q_{cc,(i,i+1)}$ are the rate of heat transfer by conduction from the cell index number (i) to the cells index numbers ($i - 1$) and ($i + 1$) respectively and, $Q_{ku,(i,i)}$ and $Q_{ku,(i,i+1)}$ are the rate of heat removed by surface convection by the cooling channels with index numbers (i) and ($i + 1$) respectively from the cell with index number (i). A schematic of the model heat transfer modes is shown in Fig. 11. A schematic with the model nomenclature is shown in Fig. 12.

The energy balance equation for the air stream flowing through the cooling channel (index number i), is given by.

$$Q_{ku,(i-1,i)} + Q_{ku,(i,i)} - Q_{u,i} = 0 \tag{29}$$

where: $(1 \le i \le N + 1)$, $Q_{ku,(i-1,i)}$ and $Q_{ku,(i,i)}$ are the heat transferred by surface conduction from cells index number (i) and (i−1) to channel (index number i) respectively, and $Q_{u,i}$ is the heat removed from cooling channel (index number i) by convection.

The rate of heat generation for a single battery cell is approximated using Equation (4). The rate of heat transfer by conduction from cell index number (i) to cells index number (i-1) and ($i + 1$) can be expressed using the conduction thermal resistance of the material located between two cells R_{cc}, as given by:

$$\begin{aligned} Q_{cc,(i,i-1)} &= \begin{cases} 0 & \text{for} \quad i = 1 \\ \dfrac{T_i - T_{i-1}}{R_{cc}} & \text{for} \quad 1 < i \le N \end{cases} \\ Q_{cc,(i,i+1)} &= \begin{cases} \dfrac{T_i - T_{i+1}}{R_{cc}} & \text{for} \quad 1 \le i < N \\ 0 & \text{for} \quad i = N \end{cases} \end{aligned} \tag{30}$$

The rate of heat transfer by surface conduction from cell index number (i) to channels index number (i) and ($i + 1$) can be expressed using the surface convection resistance $R_{ku,i}$ and the following expression:

$$\begin{aligned} Q_{ku,(i,i)} &= \begin{cases} \dfrac{T_i - T_{ch,i}}{R_{ku,i}} & \text{for} \quad 1 \le i < N + 1 \\ 0 & \text{for} \quad i = N + 1 \end{cases} \\ Q_{ku,(i,i+1)} &= \begin{cases} \dfrac{T_i - T_{ch,i+1}}{R_{ku,(i+1)}} & \text{for} \quad 1 \le i < N + 1 \\ 0 & \text{for} \quad i = N + 1 \end{cases} \end{aligned} \tag{31}$$

where: $T_{ch,i}$ and $T_{ch,i+1}$ is the outlet air temperature for the cooling channels with index numbers (i) and ($i + 1$) respectively.

Similarly, the rate of heat transfer by surface conduction from cell index number (i−1) to channel (index number i), is given by:

$$Q_{ku,(i-1,i)} = \begin{cases} 0 & \text{for} \quad i = 1 \\ \dfrac{T_{i-1} - T_{ch,i}}{R_{ku}} & \text{for} \quad 1 < i \le N + 1 \end{cases} \tag{32}$$

where $T_{ch,i-1}$ is the outlet air temperature for the cooling channel with index number (i-1).

The heat removed from cooling channel (index number i) by convection can be expressed using the convection thermal resistance R_u, as given by:

$$Q_{u,i} = \frac{T_{ch,i} - T_{air,i}}{R_{u,i}} \quad for \quad 1 \le i \le N + 1 \tag{33}$$

where $T_{\mathrm{air},i}$ is the air temperature at the inlet of the channel (index number i).

A schematic of the thermal circuit diagram for a single cell upon interconnection is shown in Fig. 13.

3.2.2. Interconnected thermal element

From the previous discussion and making the reasonable assumption that the temperature at the inlet of all channels is the same ($T_{\mathrm{air},i} = T_{\mathrm{air}}$) [7], upon interconnection, the temperature change rate for a cell (index number i) is given by:

$$\frac{dT_i}{dt} = \frac{Q_{g,i}}{m_c c_{p,c}} - \frac{Q_{d,i}(T_i, T_{air}, T_{i-1}, T_{i+1})}{m_c c_{p,c}} \tag{34}$$

where $Q_{d,i}(\cdot)$ is a linear function of T_i, $T_{\rm air}$, T_{i-1} and T_{i+1}, given by:

$$Q_{d,i}(\cdot) = \alpha_{1,i}\cdot T_i + \alpha_{2,i}\cdot T_{air,i} + \alpha_{3,i}\cdot T_{i-1} + \alpha_{4,i}\cdot T_{i+1} \tag{35}$$

where, $\alpha_{1,i}$, $\alpha_{2,i}$, $\alpha_{3,i}$, $\alpha_{4,i}$, are given by Equation (50).

Therefore, the thermal interconnection element (TIE) for a module $\mathscr{P}(n_e, m_e, \mathscr{T}_e, f_{(i)\leftrightarrow(j,k)})$ is given by the following algebraic set of equations:

$$\mathbf{Q_d} = \mathbf{D}\cdot\mathbf{T} + \mathbf{E}\cdot T_{\rm air} \tag{36}$$

where, the set of inputs to the TIE are:

- $T_{\rm air}(t)\in\mathbb{R}$, is the air temperature at the deflector plate input;
- $\mathbf{T}\in(\mathbb{R}^N\times 1)$, is the vector of cells temperatures,

$$\mathbf{T}(t) = [T_1(t), T_2(t), \ldots, T_{N-1}(t), T_N(t)]^T$$

the output of the TIE is,

- $\mathbf{Q_d}(t)\in(\mathbb{R}^N\times 1)$, is the vector of rates of heat dissipated from cells,

$$\mathbf{Q_d}(t) = \left[Q_{d,1}(t), Q_{d,2}(t), \ldots, Q_{d,N-1}(t), Q_{d,N}(t)\right]^T$$

and the TIE system parameters are given by,

- $\mathbf{D}\in(\mathbb{R}^N\times\mathbb{R}^N)$, $\mathbf{E}\in\mathbb{R}^N$, are the matrices which entries are given by Equation (49) (See appendix).

3.3. Aging submodel

The aging submodel is composed of $N+1$ elements: N cell aging elements are used to predict capacity and power fade in response of cell operating conditions charge sustaining/depleting, SOC, temperature, charging rate; and a system level SOH element to predict the *pack* state of health based on knowledge of individual cells SOH, electrical topology and voltage equalization approach.

3.3.1. Aging elements

The aging dynamics for a cell (index number i) are described by Equation (21), where the interconnected stress factor vector $w_i = [SOC_{\min,i}, \text{Ratio}, CR_i, T_i]$ is used as an input for the aging submodel, and the interconnected charge throughput is given by Ah_i, see Equation (24), where $I_i(t)$ is the input current to the battery cell (index number i) is calculated using Equation (26).

The input current at cells is a highly nonlinear function of: individual cells electrical parameters, which depend on individual cells operating conditions; individual cells capacity and power SOH; as well as battery pack electrical topology and thermal management, see Equation (26). Therefore, there is not a bijective mapping from the *pack* ampere-hour throughput ($Ah_{\mathscr{P}}$) to the battery individual *cells* ampere-hour throughput (Ah_i).

3.3.2. System level SOH element

3.3.2.1. Pack capacity SOH. In a battery *pack* the available capacity depends on individual cells capacities, battery system electrical topology and voltage equalization approach [16,48]. For a string of cells in series p (Fig. 1(a)) with passive equalization (PE), where the voltage of series connected cells is balanced by dissipating the excess of energy, all the cells in the string are fully charged and discharged limited by the lowest cell capacity. Therefore, the available capacity for a string p with PE after $Ah_p > 0$ charge throughput is given by Ref. [16]:

$$S_p(Ah_p) = \min_j \quad S_j(Ah_p) \quad 1 \le j \le m_e \tag{37}$$

where $S_j(Ah_p)$ is the capacity of the j- th cell in the string after $Ah_p > 0$ charge throughput.

Similarly, for a string of cells in series p with active equalization (AE), where the voltage of series connected cells is balanced by transferring the excess of stored energy to other cells, the available pack capacity is given by the average of the cells capacities [16]. Therefore, the available capacity for a string p with AE after $Ah_p > 0$ charge throughput is given by:

$$S_p(Ah_p) = \frac{1}{m_e}\sum_{j=1}^{m_e} S_j(Ah_j) \tag{38}$$

where $S_j(Ah_j)$ is the capacity of the j- th cell in the string after $Ah_j > 0$ charge throughput.

Due to the self balancing nature of the parallel configuration, disregarding the equalization technique used, the available capacity of an element of cells in parallel s (Fig. 1(b)) is given by n_e times the average of the cells capacities. Therefore, the available capacity for an element s after $Ah_s > 0$ charge throughput is given by:

$$S_s(Ah_s) = \sum_{k=1}^{n_e} S_k(Ah_k) \tag{39}$$

where $S_k(Ah_k)$ is the capacity of the k- th cell in the element after $Ah_k > 0$ charge throughput.

Extending the concept of *cell level* SOH_C to battery *pack level*, we define the capacity SOH of a pack $\mathscr{P}(n_e, m_e, \mathscr{T}_e, VE, f_{(i)\leftrightarrow(j,k)}, \sigma)$ as the ratio of the pack available capacity at $Ah_{\mathscr{P}} > 0$ ampere-hour throughput to the pack nominal capacity $S_{0,\mathscr{P}}$, as follows.

$$SOH_{C,\mathscr{P}}(Ah_{\mathscr{P}}) = \frac{S_{\mathscr{P}}(Ah_{\mathscr{P}})}{S_{0,\mathscr{P}}} \tag{40}$$

where $S_{\mathscr{P}}(Ah_{\mathscr{P}})$ is the pack available capacity at $Ah_{\mathscr{P}}$, and the pack nominal capacity $S_{0,\mathscr{P}}$ is given by:

$$S_{0,\mathscr{P}} = n_e\cdot S_0 \tag{41}$$

where, S_0 is nominal capacity of the cells that compose the pack. Therefore, the capacity state of health of a pack $\mathscr{P}(n_e, m_e, \mathscr{T}_e, VE, f_{(i)\leftrightarrow(j,k)}, \sigma)$ at $Ah_{\mathscr{P}} > 0$ is given by Equation (44).

3.3.2.2. Pack power SOH. In a battery pack with voltage equalization, the battery pack power loss may be correlated with the pack equivalent internal resistance. For this purpose, the reasonable assumption that the OCVs of the cells in a battery pack with equalization are similar and may be consider equal is made. Therefore, we define the power state of health of a pack as the ratio of the pack equivalent internal resistance at $Ah_{\mathscr{P}} > 0$ ampere-hour throughput to the pack nominal internal resistance $R_{0,\mathscr{P}}$ as follows:

$$SOH_{R,\mathscr{P}}(Ah_{\mathscr{P}}) = \frac{R_{\mathscr{P}}(Ah_{\mathscr{P}})}{R_{0,\mathscr{P}}} \tag{42}$$

where $R_{\mathscr{P}}(Ah_{\mathscr{P}})$ is the pack equivalent resistance given and the pack nominal resistance is given by:

$$R_{0,\mathscr{P}} = \frac{m_e}{n_e}\cdot R_0 \tag{43}$$

where R_0 is the nominal internal resistance of the cells that compose the pack. Therefore, the power state of health of a pack $\mathscr{P}(n_e, m_e, \mathscr{T}_e, VE, f_{(i)\leftrightarrow(j,k)}, \sigma)$ is given by Equation (45).

3.3.2.3. *Battery pack state-of-health equations.*

$$SOH_{C,\mathscr{P}}(Ah_{\mathscr{P}}) = \begin{cases} \dfrac{1}{n_e}\displaystyle\sum_{k=1}^{n_e}\left(\min_{k=1:m_e} SOH_{C,(j,k)}\left(Ah_{(j,k)}\right)\right) & \text{for PS with PE} \\ \dfrac{1}{n_e}\displaystyle\min_{j=1:m_e}\left(\sum_{k=1}^{n_e} SOH_{C,(j,k)}\left(Ah_{(j,k)}\right)\right) & \text{for SP with PE} \\ \dfrac{1}{n_e m_e}\displaystyle\sum_{j=1}^{m_e}\sum_{k=1}^{n_e} SOH_{C,(i,j)}\left(Ah_{(j,k)}\right) & \text{for SP/PS with AE} \end{cases} \tag{44}$$

where $SOH_{C,(j,k)}$ is the capacity state of health for cell index pair (j,k) at $Ah_{(j,k)} > 0$.

$$SOH_{R,\mathscr{P}}(Ah_{\mathscr{P}}) = \begin{cases} \dfrac{n_e}{m_e}\displaystyle\sum_{j=1}^{m_e}\left(SOH_{R,(j,1)}\left(Ah_{(j,1)}\right)\Big|\Big|\cdots\Big|\Big|SOH_{R,(j,\,n_e\,-\,1)}\left(Ah_{(j,\,n_e\,-\,1)}\right)\Big|\Big|SOH_{R,(j,\,n_e)}\left(Ah_{(j,\,n_e)}\right)\right), & \text{for SP} \\ \dfrac{n_e}{m_e}\left(\displaystyle\sum_{j=1}^{m_e} SOH_{R,(j,1)}\left(Ah_{(j,1)}\right)\right)||\cdots||\left(\displaystyle\sum_{j=1}^{m_e} SOH_{R,(j,\,n_e)}\left(Ah_{(j,n)}\right)\right), & \text{for PS} \end{cases} \tag{45}$$

where $SOH_{R,(j,k)}$ is the power state of health for cell index pair (j,k) at $Ah_{(j,k)} > 0$,and the operator $||$ is defined as $SOH_1\Big|\Big|SOH_2 = \frac{SOH_1 \cdot SOH_2}{SOH_1 + SOH_2}$.

3.4. SOC and thermal balancing

The equalization of the SOCs of different cells in the pack is implemented using both passive and active voltage equalization. The voltage equalization is implemented in the model by bringing the SOC of all cells to the lowest SOC in the pack when simulating passive voltage equalization or to the average of the cells when simulating active voltage equalization. The implementation of the voltage equalization in the pack model assumes that the equalization occurs instantaneously at the end of the CC-CV charging protocol (i.e. at $t = t_{CD} + t_{CS} + t_{\text{Charging}}$, see Fig. 3). Therefore, the electrical and thermal dynamics occurring during the balancing process are not taken into account.

Additionally, to simulate a real case scenario in which the battery is thermally balanced each time the vehicle is not in operation, the battery pack is thermally balanced at the end of each driving cycle, $t = t_{CD} + t_{CS} + t_{\text{Charging}}$, by resetting the individual cell temperatures to the ambient temperature.

3.5. Battery model

Summarizing the previous discussion, a battery module $\mathscr{P}(n_e, m_e, \mathscr{T}_e, VE, f_{(i)\leftrightarrow(j,k)}, \sigma)$ can be described by dynamic system of order $5n_e m_e$ composed of the *fast dynamics* coupled with an *slow or aging dynamics* given by:

$$\begin{aligned} &\dot{x}_i(t) = \begin{bmatrix} \dot{V}_{c,i} \\ \dot{SOC}_i \\ \dot{T}_i \end{bmatrix} = \begin{bmatrix} \dfrac{-1}{R_1C_1}V_{c,i} + \dfrac{I_i}{C_1} \\ \dfrac{-I_i}{SOH_{C,i}S_{0,i}} \\ \dfrac{I_i\left(I_i SOH_{R,i} R_{0,i} - V_{c,i}\right)}{m_c c_{p,c}} - \dfrac{Q_{d,i}}{m_c c_{p,c}} \end{bmatrix} \\ &\frac{dSOH_i}{d(Ah_i)} = \begin{bmatrix} \dfrac{dSOH_{C,i}}{d(Ah_i)} \\ \dfrac{dSOH_{R,i}}{d(Ah_i)} \end{bmatrix} = \begin{bmatrix} \phi_1(w_i)\cdot Ah_i^{z-1} \\ \phi_2(w_i) \end{bmatrix} \\ &V_i = V_{oc,i} - R_i I_i - V_{c,i} \\ &Ah_i = \int_0^t \left|I_i(t)\right| dt \\ &\mathbf{I} = \mathbf{A}_{\mathscr{T}_e}^{-1}\mathbf{B}_{\mathscr{T}_e}\left[\mathbf{V_{oc}} - \mathbf{V_c}\right] + \mathbf{A}_{\mathscr{T}_e}^{-1}\mathbf{C}_{\mathscr{T}_e} I_{\mathscr{P}} \\ &\mathbf{Q_d} = \mathbf{DT} + \mathbf{E}T_{air} \\ &I_{\mathscr{P}} = \frac{P_{\mathscr{P}}}{V_{\mathscr{P}}} \\ &SOH_{C,\mathscr{P}} \text{ is given by Eq. (42)} \\ &SOH_{R,\mathscr{P}} \text{ is given by Eq. (43)} \end{aligned} \tag{46}$$

where:

- $N = n_e \cdot m_e$ is the number of cells in the pack;

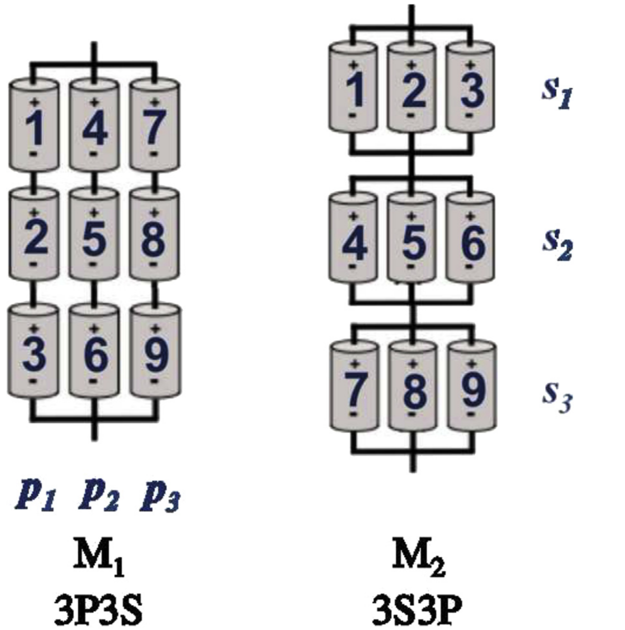

Fig. 14. Simulated battery electrical topologies: (left) Parallel strings of cells, (right) Strings of parallel cells.

- $1 \le i \le N$;
- $P_{\mathscr{P}}(t) \in \mathbb{R}$, is the input power to the pack;
- $I_{\mathscr{P}}(t) \in \mathbb{R}$, is the input current to the pack;
- $T_{air}(t) \in \mathbb{R}$, is the air temperature at the deflector plate input;
- $x_i(t) \in \mathbb{R}^3$, is the set of state variables associated with the fast dynamic behavior of cell (index number i);
- $SOH_i \in \mathbb{R}^2$, is the set of variables that described the state of health cell (index number i): the capacity state of health $SOH_{C},i(Ah_i)$; and the power state of health $SOH_{R,i}(Ah_i)$ (slowly vary with aging);
- $w_i \in \mathbb{R}^4$, are the set of stress factors for cell (index number i),

$$w_i = [SOC_{\min,i}, \mathrm{Ratio}, CR_i, T_i]$$

- $V_{\mathscr{P}} \in \mathbb{R}$, is the pack output voltage;
- $\phi_1(\cdot)$ and $\phi_2(\cdot)$ are nonlinear functions given by Equation (22);
- $I_i(t) \in \mathbb{R}$, and $Q_{d,i}(t) \in \mathbb{R}$, are the inputs acting on the cell (index number i);
- $\mathbf{I}(t) \in (\mathbb{R}^N \times 1)$, is the vector of input currents to the cells, $\mathbf{I} = [I_1, I_2, \ldots, I_{N-1}, I_N]^T$;
- $\mathbf{Q_d}(t) \in (\mathbb{R}^N \times 1)$, is the vector of heat dissipated from the cells, $\mathbf{Q_d} = [Q_{d,1}, Q_{d,2}, \ldots, Q_{d,N-1}, Q_{d,N}]^T$;
- $\mathbf{V_{oc}}(t) \in (\mathbb{R}^N \times 1)$, is the vector of cells OCV, $\mathbf{V_{oc}} = [V_{oc,1}, V_{oc,2}, \ldots, V_{oc,N-1}, V_{oc,N}]^T$;
- $\mathbf{T}(t) \in (\mathbb{R}^N \times 1)$, is the vector temperature at cells

$$\mathbf{T} = [T_1, T_2, \ldots, T_{N-1}, T_N]^T$$

- $\mathbf{V_c}(t) \in (\mathbb{R}^N \times 1)$, is the vector of cells voltages across the capacitor, $\mathbf{V_c} = [V_{c,1}, V_{c,2}, \ldots, V_{c,N-1}, V_{c,N}]^T$;
- $\mathbf{D} \in (\mathbb{R}^N \times \mathbb{R}^N)$, $\mathbf{E} \in \mathbb{R}^N$, are the matrices given by Equation (49);
- $\mathbf{A}_{\mathscr{T}_e}(\sigma, \mathbf{SOH_R}) \in (\mathbb{R}^N \times \mathbb{R}^N)$, $\mathbf{B}_{\mathscr{T}_e} \in (\mathbb{R}^N \times \mathbb{R}^N)$, $\mathbf{C}_{\mathscr{T}_e} \in \mathbb{R}^N$ are the matrices given by,

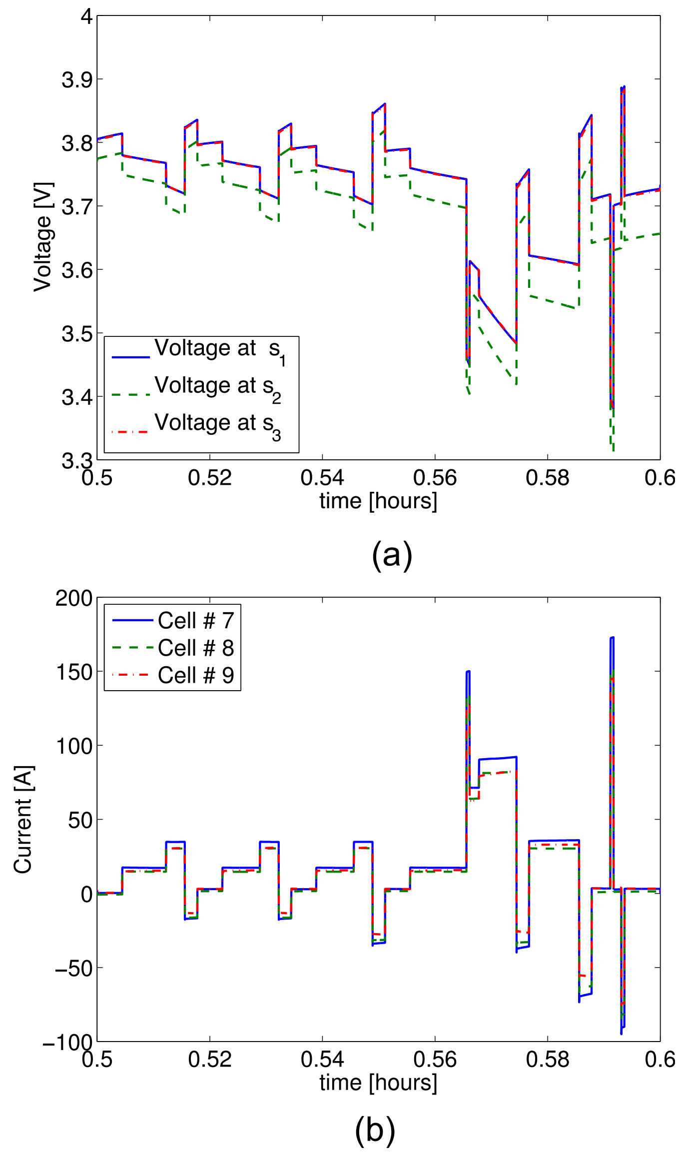

Fig. 15. (a) Voltage variation at cells in elements in series (s_1,s_2,s_3) and (b) Current variation at s_3 during a CD micro-cycle for pack $M_{2,\sigma=0.05}$ (topology 3S3P).

$$(\mathbf{A}_{\mathscr{T}_e}, \mathbf{B}_{\mathscr{T}_e}, \mathbf{C}_{\mathscr{T}_e}) = \begin{cases} \text{Equations (47)} & \text{if } \mathscr{T}_e = SP \\ \text{Equations (48)} & \text{if } \mathscr{T}_e = PS \end{cases}$$

Table 1
NMC-LMO Lithium-ion battery cell specifications.

	Value (without laminated coat)	Value (with laminated coat)
Length	0.19 [m]	0.225 [m]
Width	0.145 [m]	0.165 [m]
Thickness	5×10^{-3} [m]	
Mass	384 [g]	
Nominal capacity	15 [Ah]	
Nominal voltage	3.75 [V]	
c_p	800 $\mathrm{Jkg^{-1}\,K^{-1}}$	

Table 2
Initial cell to cell variability for simulation of packs $M_{1,\sigma=0.025}$ and.$M_{2,\sigma=0.025}$

Cell#	Capacity variability[a] $r_{C,i}$	Initial capacity $S_{0,i}$ [Ah]	Resistance variability[a] $r_{R,i}$
1	1.0138	15.2064	0.9999
2	1.0193	15.2895	1.0192
3	1.0011	15.0161	0.9904
4	0.9814	14.7203	1.0046
5	0.9907	14.8608	0.9972
6	0.9867	14.8010	1.0140
7	1.0294	15.4407	0.9864
8	0.9923	14.8846	1.0004
9	1.0094	15.1403	1.0069

[a] $r_{C,i} = N(1, 0.0125)$, $r_{R,i} = N(1, 0.0125)$, see Equation (25).

4. Simulation results

In this section, simulation results are presented and discussed. The model developed in Section 3 is used to describe two battery modules composed of $N = 9$ cells each one. The battery cells are pouch cells with composite LMO-NMC positive electrode and graphite negative electrode, for which an experimentally validated fast and slow dynamic model has been developed [23]. Each cell has a nominal capacity of 15 Ah and a nominal voltage 3.75 V, dimensions and other cell properties are presented in Table 1. The first module $(M_{1,\sigma})$ is such that $\mathscr{P}_{M_{1,\sigma}}(n_e, m_e, \mathscr{T}e, f_{(i)\leftrightarrow(j,k)}, \sigma) = (3, 3, PS, f_{M_1}, \sigma)$, while the second module $(M_{2,\sigma})$, is such that $\mathscr{P}_{M_{2,\sigma}}(n_e, m_e, \mathscr{T}e, f_{(i)\leftrightarrow(j,k)}, \sigma) = (3, 3, PS, f_{M_2}, \sigma)$. Where, the bijective mapping functions f_{M_1} and f_{M_2} are defined as shown in Fig. 14. Both packs with an air cooling arrangement as the one shown in Fig. 12. Since the pack is composed of 9 cells, the reasonable assumption that all channels are identical is made, see Ref. [7] (cooling arrangement configuration Type IV). Two simulators are developed in Matlab one for each topology.

Simulation results of the two packs under different initial cell-

Table 3
Initial cell to cell variability for simulation of packs $M_{1,\sigma=0.05}$ and.$M_{2,\sigma=0.05}$

Cell#	Capacity variability[a] $r_{C,i}$	Initial capacity S_0 [Ah]	Resistance variability[a] $r_{R,i}$
1	1.0550	15.82	0.9997
2	1.0772	16.16	1.0766
3	1.0043	15.06	0.9615
4	0.9254	13.88	1.0186
5	0.9629	14.44	0.9887
6	0.9469	14.20	1.0559
7	1.1175	16.76	0.9455
8	0.9692	14.54	1.0016
9	1.0374	15.56	1.0276

[a] $r_{C,i} = N(1, 0.05)$, $r_{R,i} = N(1, 0.05)$, see Equation (25)

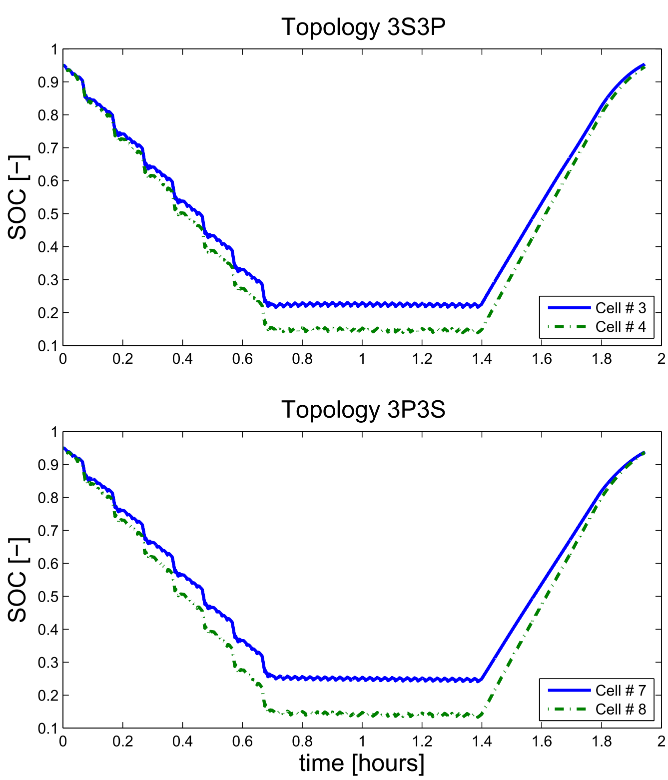

Fig. 16. State of charge profiles of the cells with the highest and lowest SOC in packs $M_{1,\sigma=0.05}$ and $M_{2,\sigma=0.05}$ during a cycle of Ratio = 0.5, SOC_{min} = 25% and CR = 3C/2, T = 15 °C.

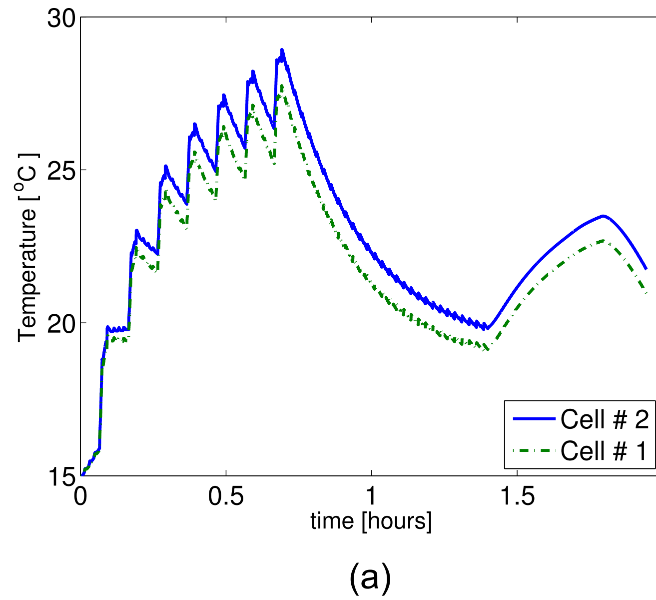

Fig. 17. Temperature transient of the hottest and coldest cells in packs (a) $M_{1,|\sigma=0.05}$ and (b) $M_{2,\sigma=0.05}$ during a cycle of Ratio = 0.5, SOC_{min} = 25%, CR = 3C/2, and T = 15 °C.

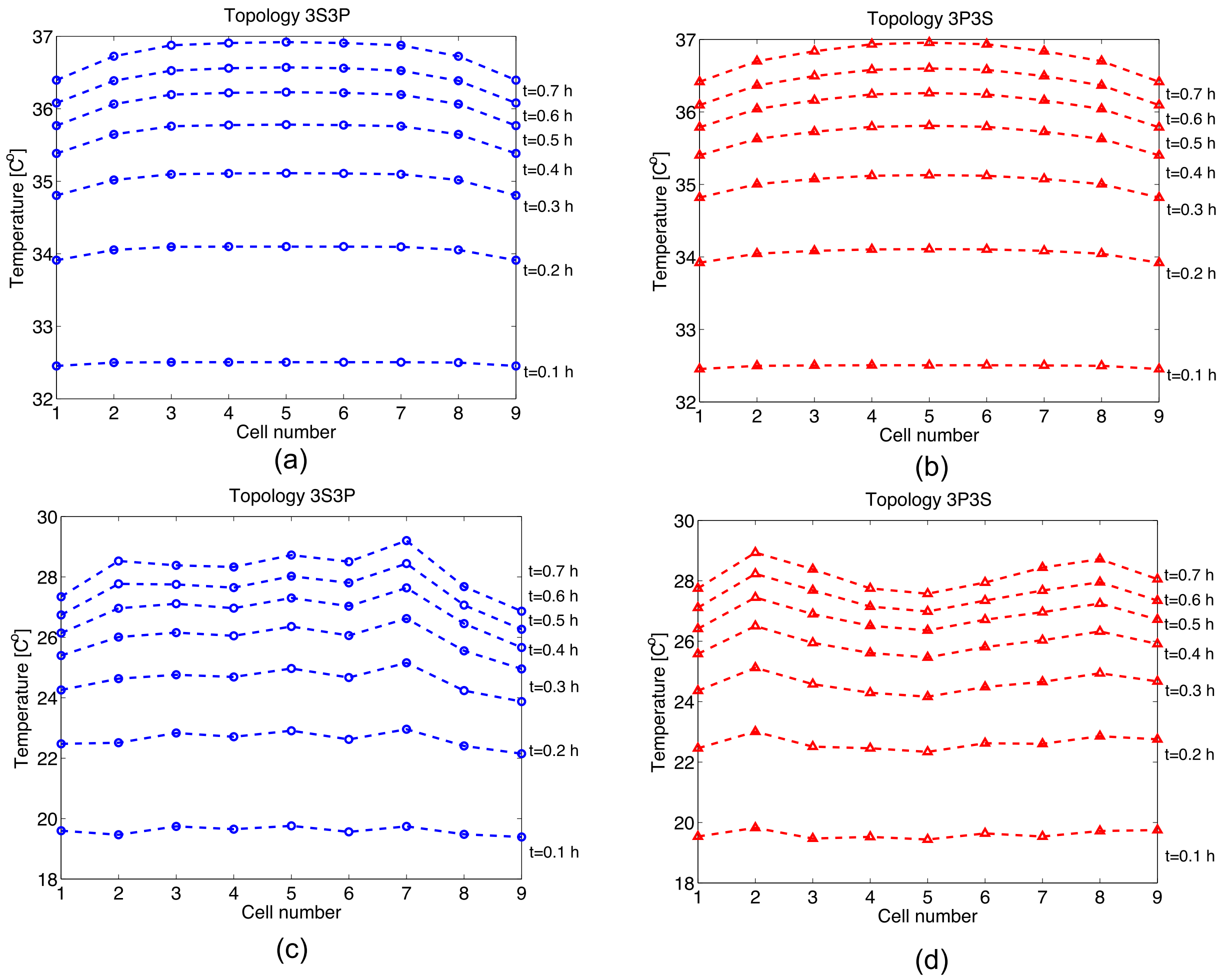

Fig. 18. Temperature variation at cells during a cycle of Ratio = 0.5, SOC_{min} = 25%, CR = 3C/2: (a) $M_{1,\sigma=0}$, T = 25 °C; (b) $M_{2,\sigma=0}$, T = 25 °C; (c) $M_{1,\sigma=0.05}$, T = 15 °C; (b) $M_{2,\sigma=0.05}$, T = 15 °C.

to-cell variability are presented. When the standard deviation of $\sigma = 0$, the initial capacity and internal resistance of all cells in the pack are identical. For the other cases, to facilitate the comparison of the results, a random set of initial conditions is generated as follows: first, a set of numbers $\mathcal{N}(0,1)$ is generated, then this set is multiplied by 0.025 or 0.05 respectively, and the nominal cell parameters are modified accordingly. The initial capacity and resistance values for the simulation results presented in this paper are shown in Tables 2 and 3.

To compare the fast and slow dynamics of a single cell to the behavior of the cells in a battery module (i.e. interconnected cells vs. not interconnected), we use nominally the same cycle conditions for both scenarios. To have nominally the same cycling conditions, the charge depleting and charge sustaining micro-cycles shown in Fig. 4, which are defined for a single cell, are scale up in such a way that if all the cells in the pack were identical, and subject to the same operational conditions, each cell would be subject to the same power cycling as the single cell. This convention is used throughout the simulation results.

4.1. Battery pack electrical dynamics

Fig. 15(a) shows the voltage variation at the elements in series (s_1,s_2,s_3) while Fig. 15(b) shows the current variation at the third element in series (s_3, cells # 7,8 and 9) for module $M_{2,\sigma=0.05}$ during ta CD micro-cycle.

Fig. 16 shows the state of charge profiles of the cells with the highest and lowest SOC in packs $M_{1,\sigma=0.05}$ and $M_{2,\sigma=0.05}$ during a cycle of Ratio = 0.5, SOC_{min} = 25%, CR = 3C/2 and T = 15 °C. Due to the self-balancing nature of the parallel configuration of elements (s_1,s_2,s_3) in $M_{1,\sigma}$, the SOC imbalance is lower for $M_{1,\sigma=0.05}$ compared to $M_{2,\sigma=0.05}$.

4.2. Battery pack thermal dynamics

Fig. 17 shows the temperature profile of the hottest and coldest cells in packs $M_{1,\sigma=0.05}$ and $M_{2,\sigma=0.05}$ during a cycle of Ratio = 0.5, SOC_{min} = 25%, CR = 3C/2, T = 15 °C. The difference between the maximum and minimum temperatures is greater for pack $M_{2,\sigma=0.05}$ for which the electrical topology allow a higher cell-to-cell current imbalance; and therefore a higher cell-to-cell heat generation imbalance compared to $M_{1,\sigma=0.05}$.

Fig. 18 (a,b) show the battery pack temperature variation at cells over time for packs $M_{1,\sigma=0}$ and $M_{2,\sigma=0}$ during a cycle of Ratio = 0.5, SOC_{min} = 25%, CR = 3C/2, T = 25 °C. Similarly, Fig. 18(c,d) show the battery pack temperature variation at cells over time for packs $M_{1,\sigma=0.05}$ and $M_{2,\sigma=0.05}$ during the same cycle at T = 15 °C. When the nominal capacity and resistance of all the cells in the pack are identical ($\sigma = 0$), and no aging has taken place, the temperature variation at cells is similar for the two topologies. However, when

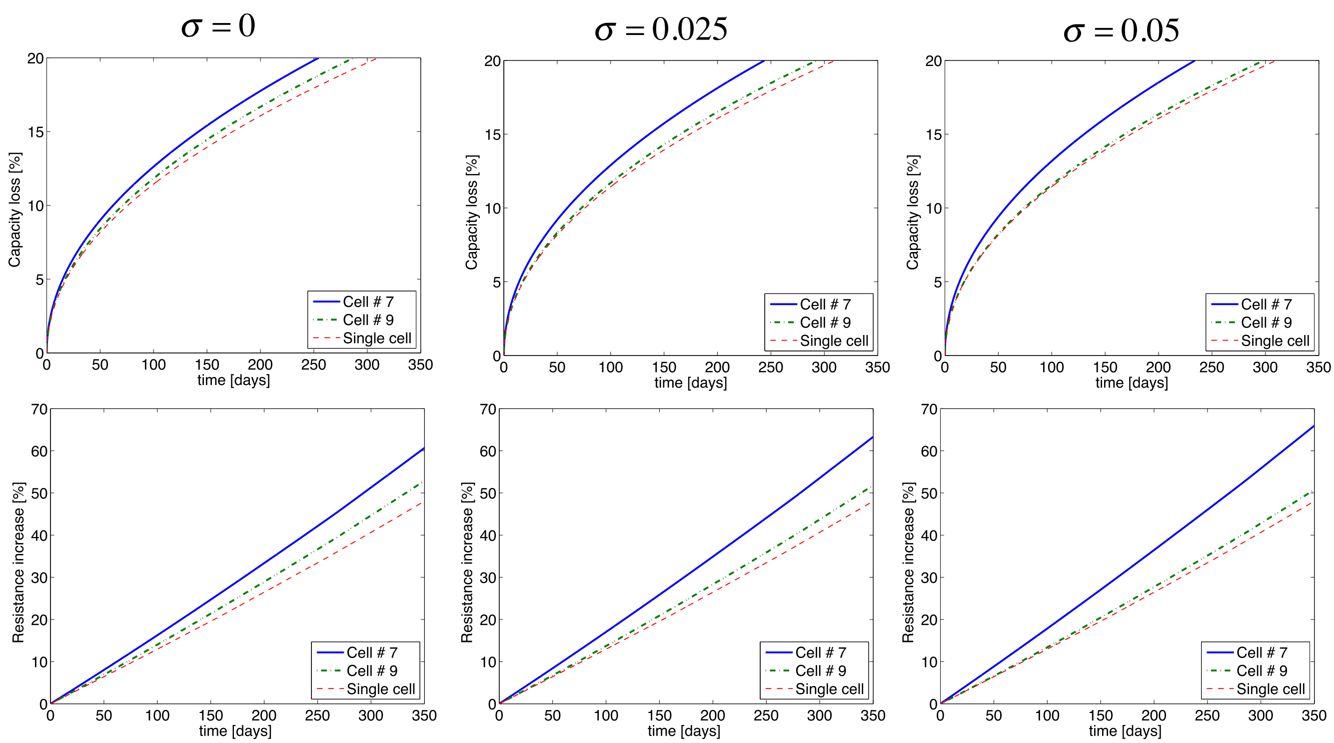

Fig. 19. Capacity loss and resistance growth evolution of the most and least aged cells compared to an isolated cell (i.e not interconnected) under the same nominal conditions for pack topology 3*S*3*P* during cycling under a Ratio = 1, SOC_{min} = 45% and CR = 3C/2 profile, T = 15 °C.

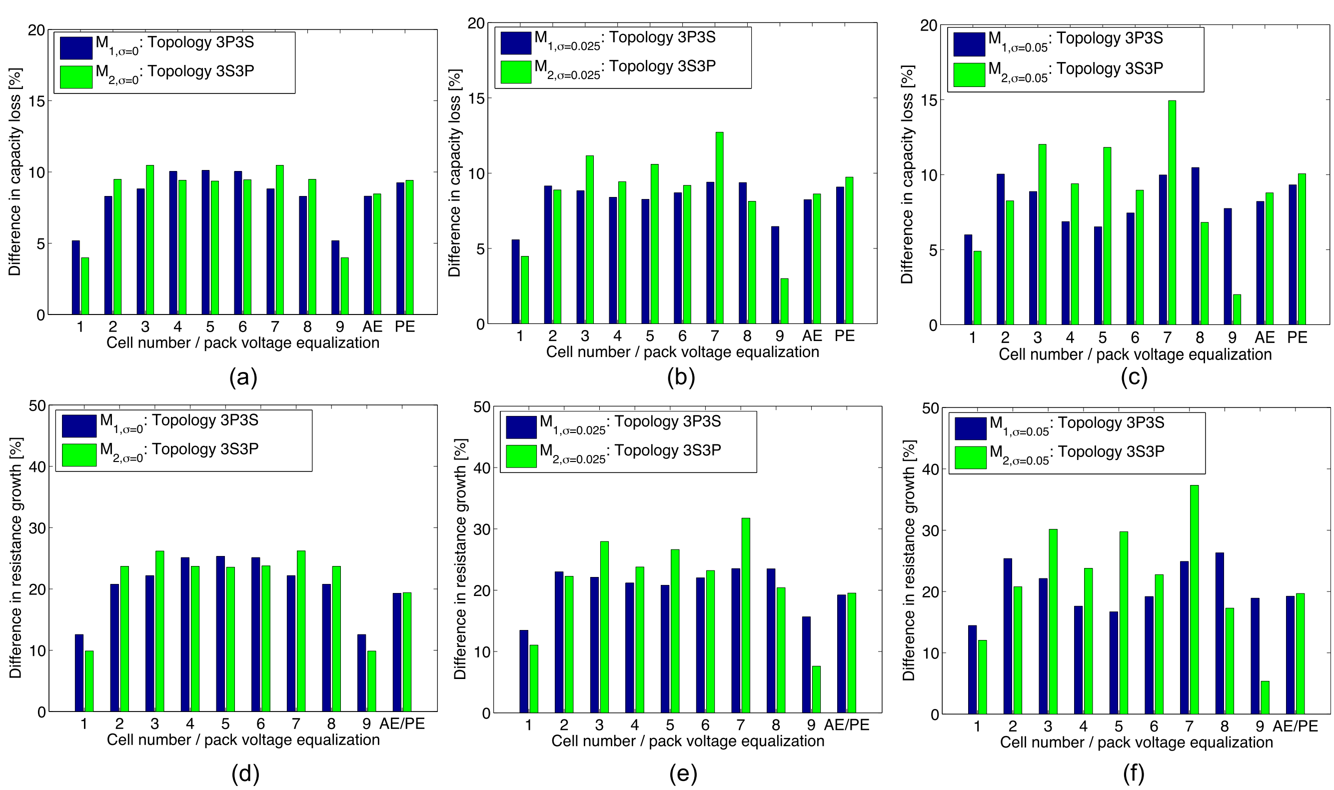

Fig. 20. Difference in the capacity loss and resistance increase attained at cells and packs M_1 and M_2 with compared to single cell at t = 310 days of continuous cycling under a nominal cycle of Ratio = 1, SOC_{min} = 45% and CR = 3C/2, T = 15 °C.

cell-to-cell manufacturing variability is considered, the temperature variation in the pack strongly depends on electrical topology. The temperature variation at cells is greater for topology $M_{2,\sigma}$ for which its electrical topology allows a higher cell-to-cell current imbalance, and therefore a higher cell-to-cell heat generation imbalance.

4.3. Battery pack aging dynamics

Fig. 19 show the capacity loss and resistance increase profiles of the most and least aged cells in packs $M_{2,\sigma=0}$, $M_{2,\sigma=0.025}$, $M_{2,\sigma=0.05}$ compared to an isolated cell (i.e not interconnected) under a cycling of Ratio = 1, SOC_{min} = 45%, CR = 3C/2, T = 15 °C. As shown in the Figures, all the cells in the pack age faster compared to the single cell reducing the battery *system* life-span. Similarly, Fig. 20 show bar plots with the difference in the capacity loss attained at *cells* and *pack* compared to an isolated cell at the same nominal cycling conditions when the isolated cell has reached its end-of-life (20% in capacity fade, approximately t = 310 days of continuous cycling. The first columns in the x axes of each bar plot correspond to the *cell* number position within the pack (see Fig. 14) while the last two columns correspond to the *pack* under active equalization (AE) and passive equalization (PE). The difference in capacity loss is expressed in percentage compared to the capacity loss attained by the isolated cell at t = 310 days (20% of capacity loss). For example, the capacity loss attainted by cell #7 in pack $M_{2,\sigma=0.05}$ at t = 310 days is approximately 23% (15% more compared to the isolated cell).

The simulation results suggest that the capacity and power fade *cell-to-cell* imbalance (i.e. aging imbalance) increases while increasing the manufacturing standard deviation (σ). The results also suggest that the distribution of the *cell-to-cell* aging imbalance depends on the pack electrical topology. The *pack* difference in capacity loss and internal resistance increase depend on the *cell-to-cell* aging imbalance as well as on the voltage equalization approach. However, the simulation results suggest that the influence of the manufacturing standard deviation (σ) on the *pack* aging is not significant. This latter statement requires an in-depth analysis as it may imply that stringent requirements currently imposed for the manufacturing of the battery cells may be possibly reduced, reducing the *battery system* cost.

5. Conclusions

The propagation of aging, which has a profound effect on battery system life-span, depends on battery electrical topology, thermal management system, cell-to-cell manufacturing variability and voltage equalization technique. This paper proposed a novel methodology for modeling aging propagation in battery packs. The methodology describes the propagation of aging and its effect on the life-span of advanced energy storage systems using a control oriented representation. The model is able to predict battery pack aging, thermal, and electrical dynamics under actual PHEV operational conditions. The model includes consideration of random variability of the cells, electrical topology and thermal management. The proposed model allow for a more complete understanding of the impacts and trade-offs of cell-to-cell variability, electrical topology and battery thermal management, on battery performance and life under actual PHEV operation.

Disclaimer

Any opinions, findings, and conclusions or recommendations expressed in this material are those of the author(s) and do not necessarily reflect the views of the National Science Foundation. This report was prepared as an account of work sponsored by an agency of the United States Government. Neither the United States Government nor any agency thereof, nor any of their employees, makes any warranty, express or implied, or assumes any legal liability or responsibility for the accuracy, completeness, or usefulness of any information, apparatus, product, or process disclosed, or represents that its use would not infringe privately owned rights. Reference herein to any specific commercial product, process, or service by trade name, trademark, manufacturer, or otherwise does not necessarily constitute or imply its endorsement, recommendation, or favoring by the United States Government or any agency thereof. The views and opinions of authors expressed herein do not necessarily state or reflect those of the United States Government or any agency thereof.

Acknowledgments

This material is based upon work supported by the National Science Foundation under Grant Number NSF-1301238 and the Department of Energy under Award Number DE-PI0000012.

Appendix

This section contains model equations, which for simplicity, were not included within the main text but are relevant components of the proposed battery pack modeling approach.

$$
\begin{aligned}
\mathbf{A}_{[l,f(j,k)]} &= \begin{cases} 1, & \text{if } (j=l),(1 \le k \le n_e),(1 \le l \le m_e) \\ R_{v,(j,k)}, & \text{if } (1 \le j \le m_e),(1 \le k \le n_e-1),(l = m_e + (j-1)(n_e-1)+k) \\ -R_{v,(j,k)}, & \text{if } (1 \le j \le m_e),(2 \le k \le n_e),(l = m_e + (j-1)(n_e-1)+(k-1)) \\ 0, & \text{else where} \end{cases} \\
\mathbf{B}_{[l,f(j,k)]} &= \begin{cases} 1, & \text{if } (1 \le j \le m_e),(1 \le k \le n_e-1),(l = m_e + (j-1)(n_e-1)+k) \\ -1, & \text{if } (1 \le j \le m_e),(2 \le k \le n_e),(l = m_e + (j-1)(n_e-1)+(k-1)) \\ 0, & \text{else where} \end{cases} \\
\mathbf{C}_{[l,1]} &= \begin{cases} 1, & \text{if } (1 \le l \le m_e) \\ 0, & \text{else where} \end{cases}
\end{aligned}
\tag{47}
$$

$$\mathbf{A}_{[l,f(j,k)]} = \begin{cases} 1, & \text{if } (j=1), (1 \le k \le n_e), (l=1) \\ 1, & \text{if } (1 \le j \le m_e - 1), (1 \le k \le n_e), (l = 1 + (k-1)(m_e-1) + j) \\ -1, & \text{if } (2 \le j \le m_e), (1 \le k \le n_e), (l = 1 + (k-1)(m_e-1) + (j-1)) \\ R_{v,(j,k)}, & \text{if } (1 \le j \le m_e), (1 \le k \le n_e - 1), (l = (1-n_e) + m_e n_e + k) \\ -R_{v,(j,k)}, & \text{if } (1 \le j \le m_e), (2 \le k \le n_e), (l = (1-n_e) + m_e n_e + (k-1)) \\ 0, & \text{else where} \end{cases}$$
$$\mathbf{B}_{[l,f(j,k)]} = \begin{cases} 1, & \text{if } (1 \le j \le m_e), (1 \le k \le n_e - 1), (l = 1 + m_e n_e - n_e + k) \\ -1, & \text{if } (1 \le j \le m_e), (2 \le k \le n_e), (l = (1-n_e) + m_e n_e + (k-1)) \\ 0, & \text{else where} \end{cases}$$
$$\mathbf{C}_{[l,1]} = \begin{cases} 1, & \text{if } (l=1) \\ 0, & \text{else where} \end{cases} \tag{48}$$

$$\mathbf{D}_{[i,j]} = \begin{cases} \alpha_{1,i} & \text{if } (1 \le i \le N), (j=i) \\ \alpha_{3,i} & \text{if } (2 \le i \le N), (j = i-1) \\ \alpha_{4,i} & \text{if } (1 \le i \le N-1), (j = i+1) \\ 0, & \text{else where} \end{cases}$$
$$\mathbf{E}_{[i,1]} = \begin{cases} \alpha_{2,i} & \text{if } (1 \le i \le N) \\ 0, & \text{else where} \end{cases} \tag{49}$$

where $\alpha_{1,i}$, $\alpha_{2,i}$, $\alpha_{3,i}$, $\alpha_{4,i}$, are given by,

$$\alpha_{1,i} = \begin{cases} \dfrac{-R_{eq,i}}{R_{ku,i}} + \dfrac{-R_{eq,i+1}}{R_{ku,i+1}} + \dfrac{1}{R_{cc,(i,i+1)}} + \dfrac{1}{R_{ku,i}} + \dfrac{1}{R_{ku,i+1}} & \text{if} \quad i = 1 \\ \dfrac{-R_{eq,i}}{R_{ku,i}} + \dfrac{-R_{eq,i+1}}{R_{ku,i+1}} + \dfrac{1}{R_{cc,(i,i+1)}} + \dfrac{1}{R_{cc,(i,i-1)}} + \dfrac{1}{R_{ku,i}} + \dfrac{1}{R_{ku,i+1}} & \text{if} \quad 2 \le i < N-1 \\ \dfrac{-R_{eq,i}}{R_{ku,i}} + \dfrac{-R_{eq,i+1}}{R_{ku,i+1}} + \dfrac{1}{R_{cc,(i,i-1)}} + \dfrac{1}{R_{ku,i}} + \dfrac{1}{R_{ku,i+1}} & \text{if} \quad i = N \end{cases}$$
$$\alpha_{2,i} = \left\{ \dfrac{-R_{eq,i}}{R_{u,i}} + \dfrac{-R_{eq,i+1}}{R_{u,i+1}} \quad \text{if} \quad 1 \le i \le N \right.$$
$$\alpha_{3,i} = \begin{cases} 0 & \text{if} \quad i = 1 \\ \dfrac{-R_{eq,i}}{R_{ku,i}} - \dfrac{1}{R_{cc,(i,i-1)}} & \text{if} \quad 2 \le i \le N \end{cases}$$
$$\alpha_{4,i} = \begin{cases} \dfrac{-R_{eq,i+1}}{R_{ku,i+1}} - \dfrac{1}{R_{cc,(i,i+1)}} & \text{if} \quad 1 \le i < N \\ 0 & \text{if} \quad i = N \end{cases} \tag{50}$$

References

[1] Anonymous, United States Department of Energy Battery Test Manual for Plug-in Hybrid Electric Vehicles, inl/ext-07-12536, rev 2 Edition, December 2010.

[2] J. Wang, P. Liu, J. Hicks-Garner, E. Sherman, S. Soukiazian, M. Verbrugge, H. Tataria, J. Musser, P. Finamore, Cycle-life model for graphite-lifepo4 cells, J. Power Sources 196 (8) (2011) 3942–3948.

[3] B. Yurkovich, Electrothermal Battery Pack Model and Simulation, The Ohio State University, 2010. M.s. theses.

[4] T.M. Bandhauer, S. Garimella, T.F. Fuller, A critical review of thermal issues in lithium-ion batteries, J. Electrochem. Soc. 158 (3) (2011) R1–R25.

[5] Z. Rao, S. Wang, A review of power battery thermal energy management, Renew. Sustain. Energy Rev. 15 (9) (2011) 4554–4571.

[6] R. Mahamud, C. Park, Reciprocating air flow for li-ion battery thermal management to improve temperature uniformity, J. Power Sources 196 (13) (2011) 5685–5696.

[7] H. Park, A design of air flow configuration for cooling lithium ion battery in hybrid electric vehicles, J. Power Sources 239 (2013) 30–36.

[8] L. Fan, J.M. Khodadadi, A.A. Pesaran, A parametric study on thermal management of an air-cooled lithium-ion battery module for plug-in hybrid electric vehicles, J. Power Sources 238 (0) (2013) 301–312.

[9] A. Jarrett, I.Y. Kim, Design optimization of electric vehicle battery cooling plates for thermal performance, J. Power Sources 196 (23) (2011) 10359–10368.

[10] Z. Rao, S. Wang, M. Wu, Z. Lin, F. Li, Experimental investigation on thermal management of electric vehicle battery with heat pipe, Energy Convers.

Manag. 65 (0) (2013) 92–97.
[11] D. Brown, R.G. Landers, Control oriented thermal modeling of lithium ion batteries from a first principle model via model reduction by the global arnoldi algorithm, J. Electrochem. Soc. 159 (12) (2012) A2043–A2052.
[12] R. Sabbah, R. Kizilel, J. Selman, S. Al-Hallaj, Active (air-cooled) vs. passive (phase change material) thermal management of high power lithium-ion packs: limitation of temperature rise and uniformity of temperature distribution, J. Power Sources 182 (2) (2008) 630–638.
[13] M. Dubarry, N. Vuillaume, B.Y. Liaw, From single cell model to battery pack simulation for li-ion batteries, J. Power Sources 186 (2) (2009) 500–507.
[14] B. Kenney, K. Darcovich, D.D. MacNeil, I.J. Davidson, Modelling the impact of variations in electrode manufacturing on lithium-ion battery modules, J. Power Sources 213 (0) (2012) 391–401.
[15] J. Cao, N. Schofield, A. Emadi, Battery balancing methods: A comprehensive review, VPPC'08, in: Vehicle Power and Propulsion Conference, 2008, IEEE, 2008, pp. 1–6.
[16] Y. Zheng, M. Ouyang, L. Lu, J. Li, X. Han, L. Xu, H. Ma, T.A. Dollmeyer, V. Freyermuth, Cell state-of-charge inconsistency estimation for lifepo4 battery pack in hybrid electric vehicles using mean-difference model, Appl. Energy 111 (0) (2013) 571–580.
[17] Y. Zheng, L. Lu, X. Han, J. Li, M. Ouyang, Lifepo4 battery pack capacity estimation for electric vehicles based on charging cell voltage curve transformation, J. Power Sources 226 (0) (2013) 33–41.
[18] C. Danielson, F. Borrelli, D. Oliver, D. Anderson, T. Phillips, Constrained flow control in storage networks: capacity maximization and balancing, Automatica 49 (9) (2013) 2612–2621.
[19] J. Kimball, B. Kuhn, P. Krein, Increased performance of battery packs by active equalization, VPPC 2007, in: Vehicle Power and Propulsion Conference, 2007, IEEE, 2007, pp. 323–327.
[20] Y.-S. Lee, M.-W. Cheng, Intelligent control battery equalization for series connected lithium-ion battery strings, Ind. Electron. IEEE Trans. 52 (5) (2005) 1297–1307.
[21] N. Kutkut, D. Divan, D. Novotny, Charge equalization for series connected battery strings, Conference Record of the 1994 IEEE, 1994, in: Industry Applications Society Annual Meeting, vol. 2, 1994, pp. 1008–1015.
[22] M. Uno, K. Tanaka, Influence of high-frequency charge -discharge cycling induced by cell voltage equalizers on the life performance of lithium-ion cells, Veh. Technol. IEEE Trans. 60 (4) (2011) 1505–1515.
[23] A. Cordoba-Arenas, S. Onori, Y. Guezennec, G. Rizzoni, Capacity and power fade cycle-life model for plug-in hybrid electric vehicles lithium-ion battery cells containing blended spinel and layered-oxide positive electrodes, J. Power Sources 278 (2015) 473–483.
[24] S.S. Zhang, The effect of the charging protocol on the cycle life of a li-ion battery, J. Power Sources 161 (2) (2006) 1385–1391.
[25] J. Vetter, P. Novák, M. Wagner, C. Veit, K.-C. Möller, J. Besenhard, M. Winter, M. Wohlfahrt-Mehrens, C. Vogler, A. Hammouche, Ageing mechanisms in lithium-ion batteries, J. Power Sources 147 (1–2) (2005) 269–281.
[26] S. Onori, P. Spagnol, V. Marano, Y. Guezennec, G. Rizzoni, A new life estimation method for lithium-ion batteries in plug-in hybrid electric vehicles applications, Int. J. Power Electron. 4 (4) (2012) 302–319.
[27] M. Wohlfahrt-Mehrens, C. Vogler, J. Garche, Aging mechanisms of lithium cathode materials, J. Power Sources 127 (1–2) (2004) 58–64.
[28] Y. Xing, N. Williard, K.-L. Tsui, M. Pecht, A comparative review of prognostics-based reliability methods for lithium batteries, in: Prognostics and System Health Management Conference (PHM-shenzhen), 2011, pp. 1–6.
[29] K. Goebel, B. Saha, A. Saxena, J. Celaya, J. Christophersen, Prognostics in battery health management, Instrum. Meas. Mag. IEEE 11 (4) (2008) 33–40.
[30] C.Y. Wang, W.B. Gu, B.Y. Liaw, Micromacroscopic coupled modeling of batteries and fuel cells: I. model development, J. Electrochem. Soc. 145 (10) (1998) 3407–3417.
[31] S. Santhanagopalan, Q. Guo, P. Ramadass, R.E. White, Review of models for predicting the cycling performance of lithium ion batteries, J. Power Sources 156 (2) (2006) 620–628.
[32] F. Todeschini, S. Onori, G. Rizzoni, An experimentally validated capacity degradation model for li-ion batteries in PHEVs application, in: 8th IFAC Symposium on Fault Detection, Supervision and Safety of Technical Processes, IFAC, 2012.
[33] I. Bloom, B. Cole, J. Sohn, S. Jones, E. Polzin, V. Battaglia, G. Henriksen, C. Motloch, R. Richardson, T. Unkelhaeuser, D. Ingersoll, H. Case, An accelerated calendar and cycle life study of li-ion cells, J. Power Sources 101 (2) (2001) 238–247.
[34] A. Cordoba-Arenas, S. Onori, R. Giorgio, G. Fan, Aging propagation in advanced battery systems: preliminary results, in: IFAC Symposium Advances in Automotive Control, Japan, September, 2013.
[35] M. Guo, R.E. White, Thermal model for lithium ion battery pack with mixed parallel and series configuration, J. Electrochem. Soc. 158 (10) (2011) A1166–A1176.
[36] H. Sun, X. Wang, B. Tossan, R. Dixon, Three-dimensional thermal modeling of a lithium-ion battery pack, J. Power Sources 206 (0) (2012) 349–356.
[37] C. Zhu, X. Li, L. Song, L. Xiang, Development of a theoretically based thermal model for lithium ion battery pack, J. Power Sources 223 (0) (2013) 155–164.
[38] V. Ramadesigan, P.W.C. Northrop, S. De, S. Santhanagopalan, R.D. Braatz, V.R. Subramanian, Modeling and simulation of lithium-ion batteries from a systems engineering perspective, J. Electrochem. Soc. 159 (3) (2012) R31–R45.
[39] G.L. Plett, Extended kalman filtering for battery management systems of lipb-based hev battery packs: part 2. modeling and identification, J. Power Sources 134 (2) (2004) 262–276.
[40] Y. Hu, S. Yurkovich, Y. Guezennec, B. Yurkovich, Electro-thermal battery model identification for automotive applications, J. Power Sources 196 (1) (2011) 449–457.
[41] M. Muratori, M. Canova, Y. Guezennec, A spatially-reduced dynamic model for the thermal characterisation of Li-ion battery cells, Int. J. Veh. Des. 58 (2) (2012) 134–158.
[42] D. Bernardi, E. Pawlikowski, J. Newman, A general energy balance for battery systems, J. Electrochem. Soc. 132 (1) (1985) 5–12.
[43] S. Kakac, Y. Yener, Convective Heat Transfer, CRC Press, 1995.
[44] Y.S. Choi, D.M. Kang, Prediction of thermal behaviors of an air-cooled lithium-ion battery system for hybrid electric vehicles, J. Power Sources 270 (0) (2014) 273–280.
[45] X. Lin, H.E. Perez, J.B. Siegel, A.G. Stefanopoulou, Y. Li, R.D. Anderson, Y. Ding, M.P. Castanier, Online Parameterization of Lumped Thermal Dynamics in Cylindrical Lithium Ion Batteries for Core Temperature Estimation and Health Monitoring, 2012.
[46] J. Payne, S. Niedzwiecki, M andKetkar, I. Isayev, Thermal characterization and management of PHEV battery packs, SAE Technical Paper 2009-01-3069.
[47] L. Serrao, S. Onori, G. Rizzoni, Y. Guezennec, Model based strategy for estimation of the residual life of automotive batteries, in: 7th IFAC Symposium on Fault Detection, Supervision and Safety of Technical Processes, IFAC, 2009, pp. 923–928.
[48] L. Lu, X. Han, J. Li, J. Hua, M. Ouyang, A review on the key issues for lithium-ion battery management in electric vehicles, J. Power Sources 226 (0) (2013) 272–288.